CHEMISTRY
A EUROPEAN JOURNAL

# Molecular and Electronic Structure of Four- and Five-Coordinate Cobalt Complexes Containing Two *o*-Phenylenediamine- or Two *o*-Aminophenol-Type Ligands at Various Oxidation Levels: An Experimental, Density Functional, and Correlated ab initio Study**

**Eckhard Bill, Eberhard Bothe, Phalguni Chaudhuri, Krzysztof Chlopek, Diran Herebian, Swarnalatha Kokatam, Kallol Ray, Thomas Weyhermüller, Frank Neese,* and Karl Wieghardt*[a]**

**Abstract:** The bidentate ligands *N*-phenyl-*o*-phenylenediamine, $H_2(^2L_N^{IP})$, or its analogue 2-(2-trifluoromethyl)-anilino-4,6-di-*tert*-butylphenol, $(^4L_O^{IP})$, react with $[Co^{II}(CH_3CO_2)_2]\cdot 4H_2O$ and triethylamine in acetonitrile in the presence of air yielding the square-planar, four-coordinate species $[Co(^2L_N)_2]$ (**1**) and $[Co(^4L_O)_2]$ (**4**) with an $S=1/2$ ground state. The corresponding nickel complexes $[Ni(^4L_O)_2]$ (**8**) and its cobaltocene reduced form $[Co^{III}(Cp)_2][Ni(^4L_O)_2]$ (**9**) have also been synthesized. The five-coordinate species $[Co(^2L_N)_2(t\text{Bu-py})]$ (**2**) ($S=1/2$) and its one-electron oxidized forms $[Co(^2L_N)_2(t\text{Bu-py})](O_2CCH_3)$ (**2a**) or $[Co(^2L_N)_2I]$ (**3**) with diamagnetic ground states ($S=0$) have been prepared, as has the species $[Co(^4L_O)_2(CH_2CN)]$ (**7**). The one-electron reduced form of **4**, namely $[Co(Cp)_2][Co(^4L_O)_2]$ (**5**) has been generated through the reduction of **4** with $[Co(Cp)_2]$. Complexes **1**, **2**, **2a**, **3**, **4**, **5**, **7**, **8**, and **9** have been characterized by X-ray crystallography (100 K). The ligands are non-innocent and may exist as catecholate-like dianions $(^2L_N^{IP})^{2-}$, $(^4L_O^{IP})^{2-}$ or π-radical semiquinonate monoanions $(^2L_N^{ISQ})^{\cdot -}$, $(^4L_O^{ISQ})^{\cdot -}$ or as neutral benzoquinones $(^2L_N^{IBQ})^0$, $(^4L_O^{IBQ})^0$; the spectroscopic oxidation states of the central metal ions vary accordingly. Electronic absorption, magnetic circular dichroism, and EPR spectroscopy, as well as variable temperature magnetic susceptibility measurements have been used to experimentally determine the electronic structures of these complexes. Density functional theoretical (DFT) and correlated ab initio calculation have been performed on the neutral and monoanionic species $[Co(^1L_N)_2]^{0,-}$ in order to understand the structural and spectroscopic properties of complexes. It is shown that the corresponding nickel complexes **8** and **9** contain a low-spin nickel(II) ion regardless of the oxidation level of the ligand, whereas for the corresponding cobalt complexes the situation is more complicated. Spectroscopic oxidation states describing a $d^6$ ($Co^{III}$) or $d^7$ ($Co^{II}$) electron configuration cannot be unambiguously assigned.

**Keywords:** ab initio calculations · cobalt · density functional calculations · nickel · radical ions

## Introduction

In 1966 Balch and Holm[1] reported that the reaction of *o*-phenylenediamine with $CoCl_2\cdot 6H_2O$ (or $[Co(CH_3CO_2)_2]\cdot 4H_2O$[2]) in the ratio 2:1 in an aqueous ammonia affords, in the presence of air, a deep violet precipitate of $[Co\{C_6H_4(NH)_2\}_2]$, which we will abbreviate here as $[Co(^1L_N)_2]$ according to Scheme 1. The room-temperature crystal structure of this complex was reported by Peng et al.[3] in 1985 (see Figure 1). The neutral, mononuclear complex is square planar; it is paramagnetic and possesses an $S=1/2$ ground state as was established by its X-band EPR spectrum and magnetochemistry.[1]

In the above reports[1–3] the authors have suggested that both organic ligands are identical and that they are mono-

[a] Dr. E. Bill, Dr. E. Bothe, Prof. Dr. P. Chaudhuri, K. Chlopek, Dr. D. Herebian, S. Kokatam, K. Ray, Dr. T. Weyhermüller, Dr. F. Neese, Prof. Dr. K. Wieghardt
Max-Planck-Institut für Bioanorganische Chemie
Stiftstrasse 34–36, 45470 Mülheim an der Ruhr (Germany)
Fax: (+49) 208-306-3952
E-mail: wieghardt@mpi-muelheim.mpg.de

[**] In this paper we use the following ligand abbreviations: the aromatic dianion, a diiminophenolate(2−), $[C_6H_4(NH)_2]^{2-}$ is $(^1L_N^{IP})^{2-}$; its π radical monoanion, a diiminosemiquinonate(1−), $[C_6H_4(NH)_2]^{\cdot -}$ is $(^1L_N^{ISQ})^{1-}$, and the neutral, diamagnetic diiminobenzoquinone form $[C_6H_4(NH)_2]^0$ is $(^1L_N^{IBQ})^0$. In cases in which the oxidation level of the ligand is not established or of relevance but its chemical composition is $[C_6H_4(NH)_2]$ we will use the abbreviation $(^1L_N)$. The *o*-aminophenolato complexes $(^XL_O)$ are analoguously abbreviated. See also Scheme 1.

  DOI: 10.1002/chem.200400850 

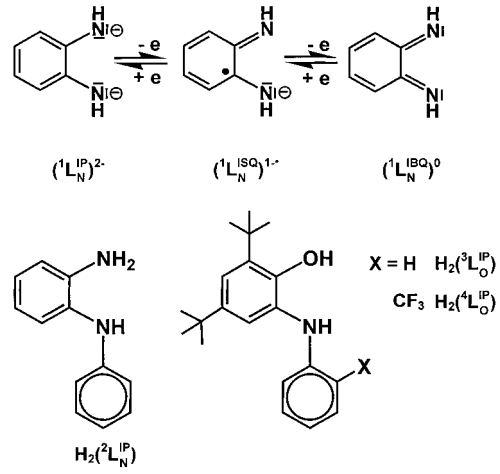


**Complexes**

| | | | |
|---|---|---|---|
| $[Co(^2L_N)_2]$ | (1) | $[CoCp_2][Co(^4L_O)_2]$ | (5) |
| $[Co(^2L_N)_2(t\text{Bu-py})]$ | (2) | $[Co(^3L_O^{ISQ})_3]$ | (6) |
| $[Co(^2L_N)_2(t\text{Bu-py})](O_2CCH_3)$ | (2a) | $[Co(^4L_O)_2(CH_2CN)]$ | (7) |
| $[Co(^2L_N)_2I]$ | (3) | $[Ni(^4L_O)_2]$ | (8) |
| $[Co(^4L_O)_2]$ | (4) | $[CoCp_2][Ni(^4L_O)_2]$ | (9) |

Scheme 1.

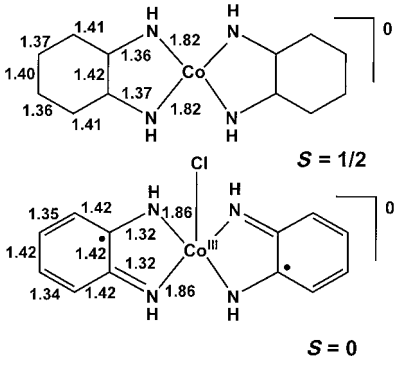


Figure 1. Schematic structures with bond lengths in Å of square-planar $[Co(^1L_N)_2]^0$ from reference [3] (top) and square-base pyramidal $[Co^{III}(^1L)_2Cl]$ from reference [3] (bottom). The experimental errors from the room-temperature crystal structures are $\sim\pm0.03$ Å ($\equiv3\sigma$) for the former and $\pm0.015$ Å for the latter.

anionic π radicals ($S_{rad}=1/2$) of the diiminobenzosemiquinonate(1−) type and that, therefore, the central cobalt ion possesses a +II oxidation state (low spin $d^7$, $S_{Co}=1/2$). In this model the spins of the ligand π radicals are assumed to be strongly intramolecularly antiferromagnetically coupled.[3]

We note that Balch and Holm suggested a different model. Using a valence-bond picture, they suggested a central low-spin cobalt(II) ion ($S=1/2$) coordinated to two closed shell $[C_6H_4(NH)_2]^{n-}$ ligands, which they formulated as two resonance hybrids between an aromatic dianion $(^1L_N^{IP})^{2-}$ and its neutral diiminobenzoquinone form $(^1L_N^{IBQ})^0$: $[Co^{II}(^1L_N^{IBQ})(^1L_N^{IP})]\rightleftarrows[Co^{II}(^1L_N^{IP})(^1L_N^{IBQ})]$. These conclusions appeared to be bolstered by the fact that 1) the corresponding highly colored, isostructural but diamagnetic complexes of $Ni^{II}$, $Pd^{II}$, and $Pt^{II}$, namely $[M(C_6H_4(NH)_2)_2]$, had also been prepared,[1] and that 2) square planar complexes of $Co^{II}$ with redox innocent ligands such as acetylacetonate(1−), (acac)[1–4] or (salen)[2–5] are known; they also possess an $S=1/2$ ground state.[6]

Even more persuasive was the observation that it is possible to oxidize $[Co(C_6H_4(NH)_2)_2]$ with air or iodine in the presence of coordinating (solvent) molecules (or anions) such as pyridine (py) or phosphines or simple halide anions ($Cl^-$, $Br^-$, $I^-$) affording diamagnetic, five-coordinate species:[1–3] $[Co^{III}(C_6H_4(NH)_2)_2X]$ (X = Cl;[2,3] I,[1,2] $SCN^-$,[2] $[Co^{III}(C_6H_4(NH)_2)_2(PPh_3)]PF_6$,[2,7] and $[Co^{III}(C_6H_4(NH)_2)_2(py)]Cl$.[8] These have in part been characterized by X-ray crystallography (Figure 1) at ambient temperature. The proposed bonding picture requires then the presence of two π radical monoanions, $(^1L_N^{ISQ})^{\cdot-}$ and an additional apical anion, X, in cases in which five-coordinate neutral species are generated or a neutral apical ligand when monocationic species are formed. In both instances the central cobalt(III) ion possesses an $S_{Co}=0$ ground state. Thus, on going from the four-coordinate to these five-coordinate species an oxidation of the central cobalt(II) to cobalt(III) is believed to occur.

It has been observed that in these diamagnetic square-base pyramidal complexes of low-spin cobalt(III) the monoanionic ligands $[C_6H_4(NH)_2]^{\cdot-}$ exhibit geometrical features that are readily ascribed to *o*-diiminosemiquinonate(1−) π radicals:[9] the average C–N bond length is in the range $1.34\pm0.01$ Å irrespective of the nature of the fifth apical ligand. Furthermore, the six-membered rings display typical quinoid type distortions with two alternating short C–C distances and four longer ones.

It is therefore quite surprising that the geometrical features of the two ligands apparently differ slightly in the four- and five-coordinate species (Figure 1). The C–N bonds are longer in the four than in the five-coordinate species (Figure 1). We note that the quality of the reported structure determinations at room temperature is not satisfactory. The average experimental error of a given C–C or C–N bond length is $\sim\pm0.03$ Å ($\equiv3\sigma$), which does not allow to safely assign an oxidation level of the ligands in the four-coordinate species. Thus, the previous authors have not been able to distinguish experimentally between the two different electronic structures **A** and **B** shown in Scheme 2 for the four-coordinate species. The difference between **A** and **B** is that **A** has *two* ligand π radicals and a central $Co^{II}$ ion ($S_{Co}=1/2$), whereas **B** may be described as a species containing a dianionic ligand, $(^1L_N^{IP})^{2-}$, and a single π radical monoanion, $(^1L_N^{ISQ})^{1-}$, as well as a $Co^{III}$ ion in a square-planar ligand field ($S_{Co}=1$). The ligand mixed valency in **B** may then be delocalized (class III) ensuring the observed structural equivalency of the two ligands on the time scale of an X-ray diffraction experiment. Model **B** would explain the longer C–N distances as a consequence of the presence of an aromatic dianion and a monoanionic π radical. In fact, one would expect the C–C and C–N distances to be the arithmetic average of the corresponding distances in the

  

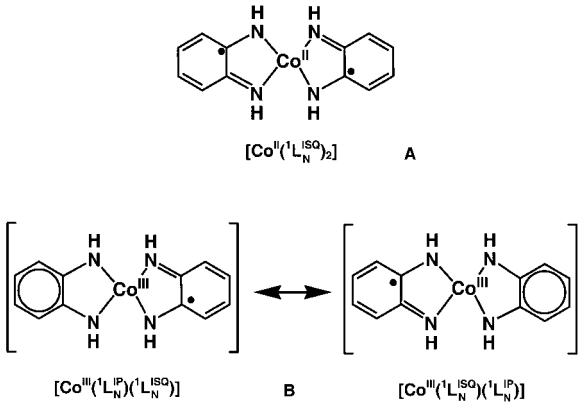


Scheme 2.

mono- and dianion, $(^1L_N^{ISQ})^{1-}$ and $(^1L_N^{IP})^{2-}$, as shown in Scheme 3. These data are quite close to the observed values of $[Co(^1L_N)_2]$ from reference [3] (Figure 1) and seem to indicate a charge distribution of this species as in $[Co^{III}(^1L_N^{IP})(^1L_N^{ISQ})]$ with charge delocalization over both ligands. The cobalt(III) ion should possess an $S_{Co}=1$ ground state as is readily deduced from ligand-field theoretical considerations ($d^6$ in a square planar field). Intramolecular antiferromagnetic coupling between the spins of the $Co^{III}$ ion and one ligand radical yields then the observed $S_t=1/2$ ground state.

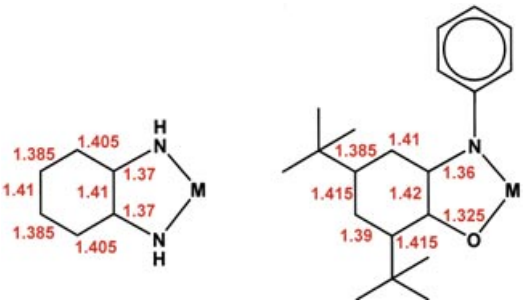


Scheme 3.

In order to clarify this ambiguity we have synthesized a series of three cobalt complexes with the ligand *N*-phenyl-*o*-phenylenediamine, $H_2(^2L_N^{IP})$. In addition, we have performed DFT and correlated ab initio theoretical calculations on neutral $[Co(^1L_N)_2]$ and its monoanion. The structure of the monocationic complex in *cis*-$[Co^{III}(^2L_N^{ISQ})_2(py)]CH_3CO_2\cdot H_2O$ has been reported by Peng et al.[10] and is shown in Figure 2. We have structurally characterized the four-coordinate species $[Co(^2L_N)_2]$ (**1**), its neutral five coordinate pyridine derivative *trans*-$[Co(^2L_N)_2(t\text{Bu-py})]^0$ (**2**), and its one-electron oxidized species *cis*-$[Co(^2L_N)_2(t\text{Bu-py})]CH_3CO_2$ (**2a**) and also the iodo complex *trans*-$[Co(^2L_N)_2I]$ (**3**).

Finally, we have used the bulky ligand 2-(2-trifluoromethyl)anilino-4,6-di-*tert*-butylphenol,[11–16] $H_2(^4L_O^{IP})$, shown in Scheme 1 and prepared the neutral four coordinate species $[Co(^4L_O)_2]$ (**4**), which is the exact analogue of **1**. It has been possible to prepare a salt of the monoanion $[Co(^4L_O)_2]^-$, namely $[Co(Cp)_2]^+[Co(^4L_O)_2]^-$ (**5**), in which $Cp^-$ is the cyclopentadienyl anion and $[Co(Cp)_2]^+$ is the cobaltocenium cation. Both **4** and **5** have been structurally characterized. Oxidation of **4** with air in acetonitrile affords $[Co(^4L_O)_2(CH_2CN)]$ (**7**). The corresponding neutral species $[Co(^4L_O)_2X]$ (X = Cl, I) have been described previously.[11] These five-coordinate complexes possess a diamagnetic central cobalt(III) ion and two $(^4L_O^{ISQ})^{\bullet-}$ radicals that are antiferromagnetically coupled yielding the observed $S=0$ ground state. Octahedral $[Co^{III}(^3L_O^{ISQ})_3]$ (**6**) possesses an $S=3/2$ ground state due to the presence of three orthogonally coordinated $(L_O^{ISQ})^{\bullet-}$ π-radical monoanions.[15] Interestingly, it has also been possible to synthesize the nickel(II)-containing complexes $[Ni^{II}(^4L_O^{ISQ})_2]$ (**8**) and its monoanionic analogue $[Co(Cp)_2][Ni^{II}(^4L_O^{IP})(^4L_O^{ISQ})]$ (**9**). As we will show here, these analogues of **4** and **5** possess different ligand oxidation levels and, concomitantly, differing spectroscopic oxidation states of the metal ions (possibly $Co^{III}$ in **4** and **5**, but certainly $Ni^{II}$ in **8** and **9**).

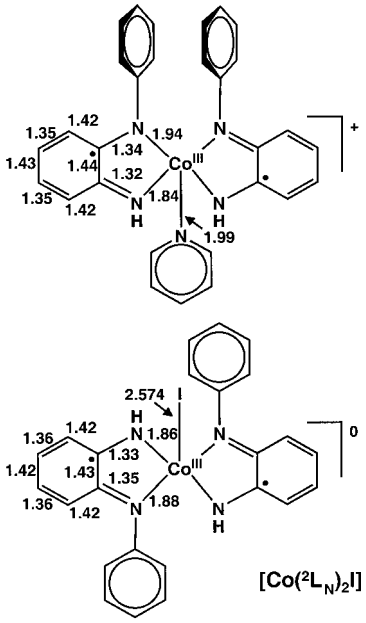


Figure 2. Schematic structures of diamagnetic five-coordinate monocation of *cis*-$[Co^{III}(^2L)_2(py)]CH_3CO_2\cdot H_2O$[10] (top) and of *trans*-$[Co^{III}(^2L)_2I]$ (**3**) of this work (bottom); the experimental error ($3\sigma$) is $\pm 0.01$ Å for the C–C, C–N distances of the former and the latter species.

Throughout this paper we carefully differentiate between formal[17] and spectroscopic (or physical)[18] oxidation states as C. K. Jörgensen proposed in 1968. A formal oxidation state of a metal ion in a given coordination compound is a non-measurable, physically meaningless, usually integral number that is derived by heterolytic removal of all ligands in their closed-shell electron configuration, whereas a spectroscopic oxidation state is derived from the actual (often observable) $d^n$ electron configuration of the metal ion in a given complex. For example, the spectroscopic oxidation state of the metal ion of a metalloprotein containing a single iron ion may be +III, since its high- or low-spin $d^5$ electron

configuration has been determined spectroscopically as such without even knowing what the ligands are (the formal oxidation state cannot be determined at this point). If redox-active, non-innocent[18] ligands are involved the formal and spectroscopic oxidation states cannot be identical.[12]

## Experimental Section

The ligand $H_2(^2L_N^{IP})$ is commercially available (Aldrich).

**2-(2-Trifluoromethyl)anilino-4,6-di-*tert*-butylphenol, $H_2(^4L_O^{IP})$**: 3,5-Di-*tert*-butylcatechol (11.1 g; 50 mmol) and 2-trifluoromethylaniline (50 mmol) were dissolved in *n*-heptane (60 mL) containing $NEt_3$ (0.5 mL). The solution was heated to reflux for 3 h in the presence of air. The volume of the colored reaction solution was reduced to ~30 mL by rotary evaporation of the solvent, whereupon a white precipitate formed that was collected by filtration and washed with a small amount of *n*-hexane. Yield: 7.6 g (43%); EI MS: *m/z* (%): 365 (100) [$M^+$], 350 (28) [$M^+-CH_3$]; elemental analysis calcd (%) for $C_{21}H_{26}NOF_3$: C 69.10, H 7.18, N 3.83; found: C 69.2, H 7.3, N 3.7.

***trans*-[Co($^2L_N$)$_2$] (1)**: [$Co(CH_3CO_2)_2$]·4$H_2O$ (0.25 g; 1.0 mmol) and $NEt_3$ (1 mL) was added to a solution of the ligand $H_2(^2L_N^{IP})$ (0.37 g; 2.0 mmol) in $CH_3CN$ (10 mL). The mixture was stirred at 20°C in the presence of air for 2 h. A deep violet microcrystalline precipitate formed that was collected by filtration, washed twice with cold $CH_3CN$ (5 mL) and dried in vacuo. X-ray quality crystals were grown by slow evaporation of the solvent of a solution of **1** in toluene under strictly anaerobic conditions. Yield: 0.34 g (81%); EI MS: *m/z*: 423 [$M^+$]; IR (KBr): $\tilde{\nu}$ = 3335, 3347 $cm^{-1}$ (NH); elemental analysis calcd (%) for $C_{24}H_{20}N_4Co$: C 68.09, H 4.76, N 13.23; found: C 68.2, H 4.9, N, 13.2.

***trans*-[Co($^2L_N$)$_2$(*t*Bu-py)] (2)**: A fiftyfold excess of 4-*tert*-butylpyridine (28.4 mmol) was added to a stirred dark blue solution of **1** (0.24 g; 0.57 mmol) in dry toluene (7 mL) under an Ar blanketing atmosphere. After 24 h of stirring at 20°C the solution was filtered. The resulting solution was allowed to stand under Ar for four months at 20°C. Dark blue-black crystals formed that were collected by filtration. Yield: 31 mg (10%); elemental analysis calcd (%) for $C_{33}H_{33}N_5Co$: C 70.96, H 5.95, N 12.54, Co 10.55; found: C 70.8, H 5.9, N 12.5, Co 10.3.

***cis*-[Co($^2L_N$)$_2$(*t*Bu-py)]$CH_3CO_2$ (2a)**: The compound has been prepared according to the published procedure for [$Co(^2L_N)_2$(py)]$CH_3CO_2$·$H_2O$.[10] Single crystals of **2a** suitable for X-ray analysis were grown from a solution of **2a** in 4-*tert*-butylpyridine into which diethyl ether was allowed to diffuse. ESI MS (pos. ion, $CH_2Cl_2$): *m/z*: 558 [$M^+$]; IR (KBr): $\tilde{\nu}$ = 3316 $cm^{-1}$ (N–H); $^1H$ NMR (300 K, $CD_2Cl_2$, 400 MHz): $\delta$ = 1.27 (s, 9H; *tert*-butyl), 1.62 (s, 3H; $CH_3CO_2$), 7.34–7.66 (m, 22H), 10.53 ppm (br s, 2H; (N–H···O)); elemental analysis calcd (%) for $C_{35}H_{36}N_5O_2Co$: C 68.06, H 5.87, N 11.34, Co 9.54; found: C 67.9, H 5.9, N 11.3, Co 9.6.

***trans*-[Co($^2L_N$)$_2$I] (3)**: This complex was prepared from a mixture of aqueous $NH_3$ (25%; 0.5 mL), the ligand $H_2(^2L_N^{IP})$ (0.18 g; 2.0 mmol) and $CH_3CN$ (10 mL) to which a solution of $CoI_2$ (0.16 g; 0.5 mmol) dissolved in $H_2O$ (5 mL) was added. The resulting solution was stirred in the presence of air for 3 h at 70°C. A dark blue precipitate formed that was collected by filtration. Single crystals suitable for X-ray crystallography were grown from a solution of **3** in THF into which diethyl ether was allowed to slowly diffuse. Yield: 0.37 g (67%); MS (EI): *m/z*: 550 [$M^+$]; IR (KBr): $\tilde{\nu}$ = 3331, 3316 $cm^{-1}$ (NH); $^1H$ NMR (300 K, $CD_2Cl_2$, 250 MHz): $\delta$ = 7.10–7.24 (m, 4H), 7.43–7.53 (m, 2H), 7.60–7.64 (m, 2H), 8.11–8.13 (m, 1H), 10.01 ppm (br s, 1H); $^{13}C\{^1H\}$ NMR (63 MHz, $CD_2Cl_2$, 300 K): $\delta$ = 119.64, 121.62, 124.60, 125.58, 125.62, 127.29, 127.72, 129.48, 130.19, 151.47, 165.28, 166.19 ppm; elemental analysis calcd (%) for $C_{24}H_{20}N_4CoI$: C 52.38, H 3.66, N 10.18, Co 10.71, I 23.06; found: C 52.46, H 3.58, N 10.12, Co 10.55, I 23.19.

**[Co($^4L_O$)$_2$] (4)**: The ligand $H_2(^4L_O^{IP})$ (2.19 g; 6 mmol) and $Co(ClO_4)_2$·$6H_2O$ (0.73 g; 2.0 mmol) were added to a deaerated solution of methanol (50 mL) and $NEt_3$ (0.8 mL). The solution was heated to reflux for 1 h and then stirred at 20°C in the presence of air for 2 h. A deep blue precipitate formed that was collected by filtration. Recrystallization from a $CH_2Cl_2/CH_3OH$ (1:1) mixture afforded single crystals suitable for X-ray crystallography. Yield: 0.81 g (54%); EI MS: *m/z* (%): 785 (100) [$M^+$]; elemental analysis calcd (%) for $C_{42}H_{48}N_2O_2F_6Co$: C 64.2, H 6.1, N 3.6, Co 7.5; found: C 64.0, H 5.9, N 3.4, Co 7.6.

**[(Cp)$_2$Co$^{III}$][Co($^4L_O$)$_2$]·2 $CH_3CN$ (5)**: [$Co(Cp)_2$] (0.19 g; 1.0 mmol) was added to a deaerated solution of **4** (0.79 g; 1.0 mmol) in $CH_2Cl_2$ (15 mL) under an Ar blanketing atmosphere. After stirring for 1 h a purple precipitate was filtered off and recrystallized from a $CH_3CN$/diethyl ether mixture (1:1). Single crystals of **5** suitable for X-ray crystallography were obtained in this fashion. Yield: 0.32 g (30%); electrospray MS ($CH_2Cl_2$) (pos. ion mode): *m/z* (%): 189 (100) [$CpCo^+$]; MS (neg. ion mode): *m/z*: 785 [$Co(^4L_O)_2^-$]; elemental analysis calcd (%) for $C_{56}H_{64}N_4F_6O_2Co_2$: C 63.69, H 6.10, N 5.30, Co 11.17; found: C 63.5, H 6.0, N 4.9, Co 10.9.

**[Co$^{III}$($^3L_O^{ISQ}$)$_3$] (6)**: This complex has been prepared as described in reference [15].

**[Co$^{III}$($^4L_O^{ISQ}$)$_2$($CH_2CN$)] (7)**: Solid $Co(ClO_4)_2$·$6H_2O$ (0.5 mmol) was added to a deaerated solution of $NEt_3$ (0.2 mL) and the ligand $H_2(^3L^{IP})$ (1.5 mmol) in $CH_3CN$ (30 mL) under an argon atmosphere. Then the solution was heated to reflux of 30 min. On cooling in the presence of air, X-ray quality black crystals of **7** precipitated. Yield: 0.25 g (60%); IR (KBr): $\tilde{\nu}$ = 2193 $cm^{-1}$ (C≡N); ESI MS (pos. ion; $CH_2Cl_2$): *m/z* (%): 785 (100) [$M^+-CH_2CN$]; elemental analysis calcd (%) for $C_{44}H_{50}F_6N_3O_2Co$: C 64.00, H 6.10, N 5.09, Co 7.14; found: C 64.0, H 6.0, N 5.1, Co 7.3.

**[Ni($^4L_O^{ISQ}$)$_2$] (8)**: This diamagnetic complex has been prepared as described for complexes **4a** or **4b** in reference [12] by using the ligand $H_2(^4L_O^{IP})$. The complex has been characterized by single-crystal X-ray crystallography (see below) for the purpose of comparison of the ligand geometrical features with those of **4** of this work. EI MS: *m/z*: 784 [$M^+-H$]; elemental analysis calcd (%) for $C_{42}H_{48}N_2O_2F_6Ni$: C 64.33, H 6.17, N 3.57, Ni 7.39; found: C 64.4, H 6.2, N 3.5, Ni 7.3.

**[Co(Cp)$_2$][Ni($^4L_O$)$_2$] (9)**: Cobaltocene (0.19 g; 1.0 mmol) was added to a degassed solution of **8** (0.79 g; 1.0 mmol) in $CH_2Cl_2$ (15 mL) under an argon blanketing atmosphere. After stirring for 3 h at 20°C a green precipitate was obtained by filtration. Yield: 0.67 g (69%); ESI MS ($CH_2Cl_2$, pos. ion): *m/z* (%): 189.2 (100) [$CoCp_2^+$]; MS (neg. ion): *m/z*: 784.6 [$Ni(^4L_O)_2^-$]; elemental analysis calcd (%) for $C_{52}H_{58}N_2O_2F_6CoNi$: C 64.20, H 6.0, N 2.88, Ni 6.0, Co 6.0; found: C 64.0, H 5.9, N 3.0, Ni 6.0, Co 6.1.

**X-ray crystallographic data collection and refinement of the structures**: A dark red single crystal of **1**, a dark brown crystal of **5**, and black crystals of **2**, **2a**, **3**, **4**, **8**, **8a**, **8b**, **8c**, and **9** were coated with perfluoropolyether and mounted in the nitrogen cold stream of a Nonius Kappa-CCD diffractometer equipped with a Mo-target rotating-anode X-ray source and a graphite monochromator ($Mo_{K\alpha}$, $\lambda$ = 0.71073 Å). All measurements were recorded at a temperature of 100(2) K. A dark red crystal of **7** was treated the same way, but was mounted on a Siemens SMART diffractometer system equipped with a Cu fine focus tube ($Cu_{K\alpha}$, $\lambda$ = 1.54178 Å). Final cell constants were obtained from least-squares fits of subsets of several thousand strong reflections. Crystal faces of **1**, **3**, **4**, **5**, **8**, **8a**, **8b**, and **8c** were determined and the corresponding intensity data were corrected for absorption using the Gaussian-type routine embedded in XPREP.[19] Data set of **7** was corrected for absorption using the program SADABS.[20] The Siemens SHELXTL[19] software package was used for solution and artwork of the structure, SHELXL97[21] was used for the refinement. The structures were readily solved by direct and Patterson methods and subsequent difference Fourier techniques. All non-hydrogen atoms were refined anisotropically. Hydrogen atoms attached to carbon atoms were placed at calculated positions and refined as riding atoms with isotropic displacement parameters. Crystallographic data of the compounds are listed in Table 1. Further details are available from the Cambridge Crystallographic Data Centre. The crystals of **8a**, **8b**, and **8c** represent polymorphs of **8** that have been obtained on various occasions. These results are given in the supplementary crystallographic data only. They will not be discussed in the text.

CCDC-243458–243468 contains the supplementary crystallographic data for complexes **1**, **2**, **2a**, **3**, **4**, **5**, **7**, **8**, **8a**–**c**, whereas CCDC-243843 contains the material for **9**. These data can be obtained free of charge via

  

Table 1. Crystallographic data for **1**, **2**, **2a**·$H_2O$, **3**·THF, **4**, **5**·2$CH_3CN$, **7**, **8**, and **9**·$CH_3CN$

| | **1** | **2** | **2a** | **3** |
|---|---|---|---|---|
| formula | $C_{24}H_{20}CoN_4$ | $C_{33}H_{33}CoN_5$ | $C_{35}H_{38}CoN_5O_3$ | $C_{28}H_{28}CoIN_4O$ |
| $M_r$ | 423.37 | 558.57 | 635.63 | 622.37 |
| space group | $P\bar{1}$ (No. 2) | $P\bar{1}$ (No. 2) | $P2_1/n$ (No. 14) | $P2_12_12_1$ (No. 19) |
| $a$ [Å] | 9.6250(6) | 10.207(2) | 15.1278(8) | 8.8007(3) |
| $b$ [Å] | 10.3004(6) | 10.862(2) | 13.0595(6) | 8.8335(3) |
| $c$ [Å] | 11.5432(8) | 13.285(3) | 15.6260(8) | 32.1615(12) |
| $\alpha$ [°] | 74.17(1) | 78.19(2) | 90 | 90 |
| $\beta$ [°] | 75.86(1) | 79.88(2) | 91.61(1) | 90 |
| $\gamma$ [°] | 62.59(1) | 74.70(2) | 90 | 90 |
| $V$ [Å$^3$] | 967.91(11) | 1379.0(5) | 3085.9(3) | 2500.3(2) |
| $Z$ | 2 | 2 | 4 | 4 |
| $\rho_{calcd}$ [g cm$^{-3}$] | 1.453 | 1.345 | 1.368 | 1.653 |
| $2\theta_{max}$ | 56.6 | 50.00 | 55.00 | 60.94 |
| reflns collected | 20688 | 8481 | 51821 | 33248 |
| unique reflns | 4796 | 4827 | 7071 | 7522 |
| observed reflns [$I>2\sigma(I)$] | 3878 | 4402 | 5420 | 6982 |
| parameters/restraints | 271/0 | 341/7 | 415/1 | 322/1 |
| $\mu$(K$\alpha$) [cm$^{-1}$] | 9.04 | 6.54 | 6.00 | 19.50 |
| $R1$[a]/GoF[b] | 0.0349/1.034 | 0.1003/1.065 | 0.0555/1.057 | 0.0374/1.078 |
| $wR2$[c] [$I>2\sigma(I)$] | 0.0745 | 0.2457 | 0.1149 | 0.0784 |
| residual density [e Å$^{-3}$] | +0.43/−0.34 | +5.07/−0.92 | +0.76/−0.44 | +1.32/−0.68 |

| | **4** | **5** | **7** | **8** | **9** |
|---|---|---|---|---|---|
| formula | $C_{42}H_{48}CoF_6N_2O_2$ | $C_{56}H_{64}Co_2F_6N_4O_2$ | $C_{44}H_{50}CoF_6N_3O_2$ | $C_{42}H_{48}F_6N_2NiO_2$ | $C_{54}H_{61}CoF_6N_3NiO_2$ |
| $M_r$ | 785.75 | 1056.97 | 825.80 | 785.53 | 1015.70 |
| space group | $P\bar{1}$ (No. 2) | $P\bar{1}$ (No. 2) | $C2/c$ (No. 15) | $P2_1/c$ (No. 14) | $P2_12_12_1$ (No. 19) |
| $a$ [Å] | 17.0501(8) | 12.3198(6) | 20.068(2) | 9.7701(6) | 10.2271(4) |
| $b$ [Å] | 17.3146(6) | 13.5850(6) | 12.8531(12) | 13.8343(8) | 20.4853(10) |
| $c$ [Å] | 18.0229(8) | 17.6577(9) | 33.765(3) | 15.2068(10) | 23.6043(14) |
| $\alpha$ [°] | 64.51(1) | 93.31(1) | 90 | 90 | 90 |
| $\beta$ [°] | 85.16(1) | 105.23(1) | 106.45(1) | 94.75(1) | 90 |
| $\gamma$ [°] | 60.78(1) | 110.58(1) | 90 | 90 | 90 |
| $V$ [Å$^3$] | 4137.9(13) | 2632.4(2) | 8352.7(14) | 2048.3(2) | 4945.2(4) |
| $Z$ | 4 | 2 | 8 | 2 | 4 |
| $\rho_{calcd}$ [g cm$^{-3}$] | 1.261 | 1.333 | 1.313 | 1.274 | 1.364 |
| $2\theta_{max}$ | 55.0 | 55.0 | 125.74 | 61.94 | 50.0 |
| reflns collected | 56392 | 35495 | 20233 | 23258 | 62008 |
| unique reflns | 18976 | 11968 | 6408 | 6485 | 8669 |
| observed reflns [$I>2\sigma(I)$] | 14329 | 10003 | 5718 | 5488 | 6489 |
| parameters/restraints | 982/0 | 676/60 | 523/1 | 247/0 | 617/0 |
| $\mu$(K$\alpha$) [cm$^{-1}$] | 4.77 | 6.96 | 37.84 | 5.37 | 7.82 |
| $R1$[a]/GoF[b] | 0.0561/1.030 | 0.0658/1.083 | 0.0760/1.214 | 0.0383/1.067 | 0.0491/1.035 |
| $wR2$[c] [$I>2\sigma(I)$] | 0.1388 | 0.1796 | 0.1470 | 0.0892 | 0.0718 |
| residual density [e Å$^{-3}$] | +1.65/−0.54 | +1.37/−1.32 | +0.57/−0.48 | +0.44/−0.37 | +0.42/−0.31 |

[a] Observation criterion: $I>2\sigma(I)$. $R1=\Sigma||F_o|-|F_c||/\Sigma|F_o|$. [b] Goodness of fit (GoF)$=[\Sigma\{w(F_o^2-F_c^2)^2\}/(n-p)]^{1/2}$. [c] $wR2=[\Sigma\{w(F_o2-F_c^2)^2\}/\Sigma\{w(F_o^2)^2\}]^{1/2}$ in which $w=1/\sigma^2(F_o^2)+(aP)^2+bP$ and $P=(F_o^2+2F_c^2)/3$.

www.ccdc.cam.ac.uk/conts/retrieving.html (or from the Cambridge Crystallographic Data Centre, 12 Union Road, Cambridge, CB2 1EZ, UK; fax (+44)223–336–033; or deposit@ccdc.cam.ac.uk).

**Physical measurements**: Electronic absorption spectra of complexes and spectra from the spectroelectrochemical measurements were recorded on HP 8452 A diode array spectrophotometer (range: 200–1700 nm). Cyclic voltammograms and coulometric electrochemical experiments were performed with an EG&G potentiostat/galvanostat. Temperature-dependent (2–298 K) magnetization data were recorded with a SQUID magnetometer (MPMS Quantum Design) in an external magnetic field of 1 T. The experimental magnetic susceptibility data were corrected for underlying diamagnetism by use of tabulated Pascal's constants. X-band EPR spectra were recorded with a Bruker ESP 300 spectrometer. Magnetic circular dichroism spectra were obtained on a home built instrument consisting of a JASCO J-715 spectropolarimeter and an Oxford Instruments SPECTROMAG magnetocryostat (generating magnetic fields of up to 11 T). Spectra were taken for samples dissolved in butyronitrile, which gave high-quality glasses suitable for optical spectroscopy at cryogenic temperatures. Simultaneous gaussian resolution of absorption and magnetic circular dichroism (MCD) spectra were performed by using the PeakFit program and *C/D* ratios were calculated by using Equation (1).

$$\frac{C}{D}=\frac{k_BT}{\mu_BB}\frac{\int\frac{\Delta\varepsilon(\nu)}{\nu}d\nu}{\int\frac{\varepsilon(\nu)}{\nu}d\nu} \quad (1)$$

Since we have determined the Gaussian fit from a spectrum recorded at 1.8 K and 5 T, the *C*/*D* ratio defined above was multiplied by a factor of 2.22 (determined from the appropriate $S=^1/_2$ simulation) in order to account for partial saturation of the signal at low temperatures and high magnetic fields.

**Calculations**: All calculations reported in this paper were done with the program package ORCA.[22] All geometry optimizations were carried out at the BP86 level[23,24] of DFT. This functional has proved in many applications its ability to reliably predict structures of transition-metal complexes. The all-electron Gaussian basis sets used were those reported by the Ahlrichs group.[25] Accurate triple-$\zeta$ valence basis sets with one set of polarization functions on the metal and nitrogen atoms were used (TZV(P)).[25b] The carbon and hydrogen atoms were described by a

slightly smaller polarized split-valence SV(P) basis sets that is of double-$\zeta$ quality in the valence region and contains a polarizing set of d-functions on the non-hydrogen atoms.[25a] The auxillary basis sets used to fit the electron density were taken from the Turbomole library[26] and were chosen to match the orbital basis. The SCF calculations were always of the spin-polarized type and were tightly converged ($10^{-7}$ Eh in energy, $10^{-6}$ Eh in the density change and $10^{-6}$ in maximum element of the DIIS[27] error vector). Single-point calculations with the B3LYP functional[23,28,29] were carried out at the optimized geometries. Ab initio calculations of the optical spectra were also undertaken with the ORCA program and utilized the recently developed spectroscopy oriented configuration interaction (SORCI) formalism.[30] In these calculations the TZVP basis set was used on the central cobalt atom and the SV(P) basis set on all other atoms. The selection threshold $T_{sel}$ was $10^{-6}$ Eh. All other parameters were default values described in reference [30]. The lowest thirteen roots were calculated for the neutral species and the lowest fourteen roots for the anion. The calculations were started with spin-restricted orbitals from BP86 DFT calculations. For the anion it turns out that the highest occupied MOs are unbound and much too diffuse. Consequently, we started the SORCI calculations for the anion from the orbitals of the neutral species obtained at the optimized geometry of the anion. The reference space were CAS(11,8) for the neutral comlex and CAS(12,8) for the anion. As described below this encompasses all important valence orbitals of both ligand and metal parentage.

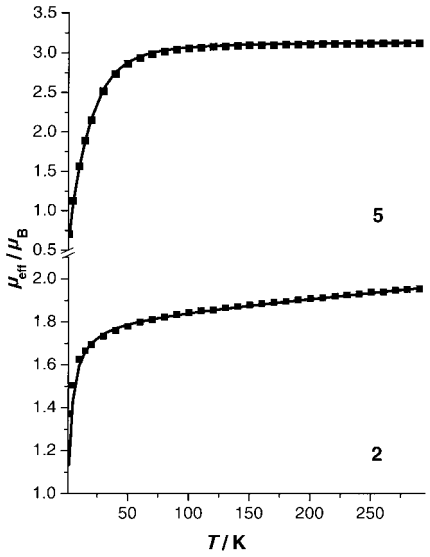


Figure 3. Temperature dependence of the magnetic moment of solid **5** (top) and **2** (bottom). The solid lines represent best fits with parameters for **5**: $S=1$; $|D|=57\ cm^{-1}$; $g=2.25$, and for **2**: $S=^1/_2$, $g_{iso}=2.09$, $\chi_{TIP}=250\times10^{-6}$ emu; $\theta=-3.0$ K.

## Results

**Syntheses and characterization**: The reaction of the ligand *N*-phenyl-*o*-phenylenediamine ($H_2(^2L_N^{IP})$) and $[Co^{II}(CH_3CO_2)_2]\cdot4H_2O$ in the ratio 2:1 in acetonitrile in the presence of the base triethylamine and air affords deep violet microcrystals of *trans*-$[Co(^2L_N)_2]$ (**1**) in excellent yield. From variable-temperature measurements of the molar magnetic susceptibility it was established that **1** possesses an $S=^1/_2$ ground state ($\mu_{eff}$ (20–298 K) = 1.9 $\mu_B$). Complex **1** displays two $\nu$(N–H) stretching frequencies at 3335 and 3347 $cm^{-1}$ (KBr disk) in the infrared region.

From an anaerobic solution of **1** in toluene, to which an excess of 4-*tert*-butylpyridine had been added under an argon blanketing atmosphere, dark blue-black crystals of the neutral adduct *trans*-$[Co(^2L_N)_2(t$Bu-py$)]$ (**2**) were obtained. In the infrared spectrum two $\nu$(N–H) modes are observed at 3335 and 3346 $cm^{-1}$. The temperature dependence of the magnetic moment of **2** is shown in Figure 3. A model comprising temperature-independent paramagnetism of $250\times10^{-6}$ emu and a Weiss constant $\theta$ of $-3$ K indicating weak intermolecular antiferromagnetic coupling, a $g_{iso}$ value of 2.09, and an $S=^1/_2$ ground state was found to yield a satisfactory fit of the data ($\mu_{eff}$ (70–298 K): 1.85 $\mu_B$).

When a mixture of the ligand $H_2(^2L_N^{IP})$ and $[Co^{II}(CH_3CO_2)_2]$ (2:1) was stirred in the presence of air in 4-*tert*-butylpyridine deep blue, diamagnetic crystals of *cis*-$[Co(^2L_N)_2(t$Bu-py$)]CH_3CO_2\cdot H_2O$ (**2a**) were obtained in good yield. The material is formally the one-electron oxidation product of **2**. Previously, the complex *cis*-$[Co^{III}(^2L_N^{ISQ})_2(py)]CH_3CO_2\cdot H_2O$ was structurally characterized at ambient temperature[10] (Figure 2).

When a solution of $CoI_2$ and the ligand $H_2(^2L_N^{IP})$ (1:2) in $CH_3CN$, to which a solution of aqueous ammonia (25%) had been added, was stirred at 70 °C in the presence of air a dark blue precipitate of $[Co(^2L_N)_2I]$ (**3**) was obtained. This material is also diamagnetic as was judged from its normal $^1H$ NMR and $^{13}C$ NMR spectra (Experimental Section). The infrared spectrum (KBr disk) shows two $\nu$(N–H) modes at 3331 and 3316 $cm^{-1}$.

By using the ligand 2-(2-trifluoromethyl)anilino-4,6-di-*tert*-butylphenol, $H_2(^4L_O^{IP})$, as starting material for its reaction with $Co(ClO_4)_2\cdot6H_2O$ (2:1) in methanol and $NEt_3$ in the presence of air deep blue crystals of $[Co(^4L_O)_2]$ (**4**) were obtained in good yield. In the temperature range 80–298 K, complex **4** displays a temperature-independent magnetic moment of 2.35 $\mu_B$ ($g=2.43$, $\chi_{TIP}=0.14\times10^{-3}$ emu) which is indicative of its $S=^1/_2$ ground state.

When a deaerated solution of **4** in $CH_2Cl_2$ reacted with one equivalent of the reductant cobaltocene, $[Co(Cp)_2]$, under argon a purple precipitate of the salt $[Co^{III}(Cp)_2][Co(^4L_O)_2]$ (**5**) was obtained. The bis(acetonitrile) salt **5**$\cdot2CH_3CN$ crystallized from $CH_3CN$. The crystal structure (see below) shows that the diamagnetic cobalticenium cation, a $[Co(^4L_O)_2]^-$ ion, and two uncoordinated acetonitrile molecules of crystallization are present. Figure 3 displays the temperature dependence of the effective magnetic moment of **5**. A satisfactory model for the data has been obtained by using the following fit parameters: $S=1$, $D=57\ cm^{-1}$, and $g=2.26$. A very similar large zero-field splitting parameter ($D=32\ cm^{-1}$) has been reported for a bis(benzodithiolato)cobalt(III) monoanion, which also has an $S=1$ ground state.[31] These results imply that the charge distribution in the monoanion is best described as $[Co^{III}(^4L_O^{IP})_2]^-$, whereby two closed-shell dianions, $(^4L_O^{IP})^{2-}$, are bound in a square-planar fashion to a cobalt(III) ion affording an $S_{Co}=1$ ground state. A number of square-planar cobalt(III) complexes with an $S=1$ ground state containing innocent N,O-donor ligands have been described in the literature.[32] These

  

complexes also display remarkably large zero-field splittings ($|D| > 50\ cm^{-1}$). This is in stark contrast to the previously reported octahedral analogue $[Co^{III}(^3L_O^{ISQ})_3]$ (**6**), which possess an $S = {}^2/_3$ ground state. This is typical for the presence of three orthogonally coordinated *o*-iminobenzosemiquinonate(1−) radicals and a diamagnetic central cobalt(III) ion.[15]

Interestingly, when the above synthesis of **4** was carried out in acetonitrile instead of methanol in the presence of air, a different crystalline, deep blue-violet (black) product was obtained, namely $[Co^{III}(^4L_O^{ISQ})_2(CH_2CN)]$ (**7**). The complex is diamagnetic ($S = 0$). The compound contains a carbon-coordinated ion $(CH_2CN)^-$. Some cobalt complexes containing such a carbon-coordinated $CH_2CN^-$ ion have been described.[33]

We have also prepared the deep blue, neutral, diamagnetic nickel(II) complex $[Ni^{II}(^4L_O^{ISQ})_2]$ (**8**) in a completely analogous fashion as described for $[Ni^{II}(^3L_O^{ISQ})_2]$ in reference [12]. The structure of **8** has been determined by X-ray crystallography at 100 K (see below) in order to compare the dimensions of the coordinated ligands with those in **4**. It has also been possible to reduce **8** by cobaltocene affording the green, paramagnetic salt $[Co(Cp)_2][Ni(^4L_O)_2]$ (**9**). The anion of complex **9** possesses an $S = {}^1/_2$ ground state ($\mu_{eff}$ (70–298 K) = 1.8 $\mu_B$) and displays a charge distribution as in $[Ni^{II}(^4L_O^{ISQ})(^4L_O^{IP})]^- \rightleftarrows [Ni^{II}(^4L_O^{IP})(^4L_O^{ISQ})]^-$.

**Crystal structures**: Figure 4 shows the C–N, C–O, and C–C bond lengths in N,N- and N,O-coordinated ligands as a function of their respective oxidation level, namely $(^2L_N^{ISQ})^{\bullet -}$ and $(^2L_N^{IBQ})^0$ in $[Pd^{II}(bpy)(^2L_N^{ISQ})]PF_6$ ($S = {}^1/_2$)[13] and $[Ru^{II}(bpy)_2(^2L_N^{IBQ})](PF_6)_2$,[10] respectively, and $(^3L_O^{IP})^{2-}$ in $[Pd^{II}(bpy)(^3L_O^{IP})]$,[14] $(^3L_O^{ISQ})^{\bullet -}$ in $[Pd^{II}(bpy)(^3L_O^{ISQ})]PF_6$,[14], and $(^3L_O^{IBQ})^0$ in $[Ni^{II}(tren)(^3L_O^{IBQ})](PF_6)_2$.[16] Clearly, the C–N, C–O, and C–C distances vary with the ligand oxidation level in a predictable manner and, conversely, the measured distances in a given complex should allow the experimental determination of the oxidation level of such a ligand in a given complex.[9] Selected bond lengths of complexes are summarized in Table 2.

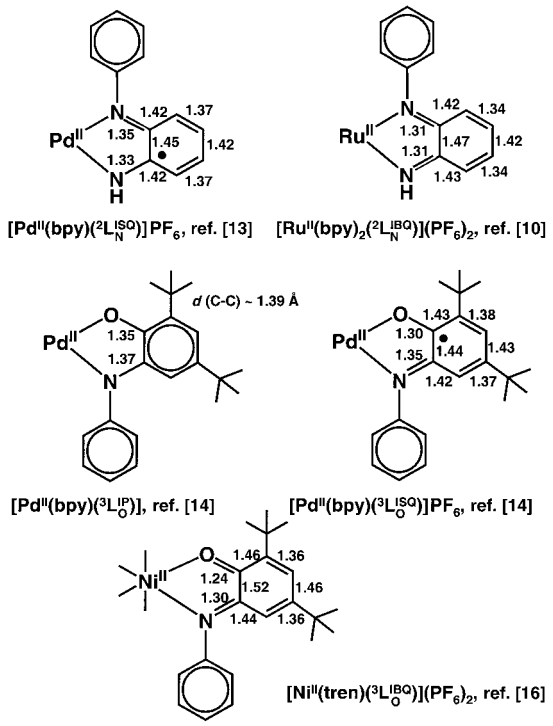


Figure 4. Average C–O, C–N, and C–C distances in Å in complexes containing $(^2L_N)^{n-}$ or $(^3L_O)^{n-}$ ligands ($n = 2-, 1-, 0$).

The structures of neutral, mononuclear $[Co(^2L_N)_2]$ (**1**), $[Co(^4L_O)_2]$ (**4**), and $[Ni(^4L_O)_2]$ (**8**) are square planar as shown in Figure 5. Average C–N and C–C bond lengths are given in Figure 6. Note that at this stage we do not assign oxidation states to the central cobalt ion or the ligands in complexes **1** and **4**, because the experimentally observed C–O, C–N, and C–C distances do not closely resemble any pattern in Figure 4. On the other hand, it is remarkable that the ligand oxidation level of the square-planar nickel complex **8** (Figure 5) is in excellent agreement with the notion that two monoanionic π-radical ligands $(^4L_O^{ISQ})^{\bullet -}$ are present and, therefore, the nickel ion possesses an experimentally determined spectroscopic oxidation state of +II ($d^8$). Very similar dimensions of the π radical ligands have been reported in reference [12] for $[M(^3L_O^{ISQ})_2]$ (M = $Ni^{II}$, $Pd^{II}$, $Pt^{II}$) complexes. Thus, the charge distribution in **8** is best described as $[Ni^{II}(^3L_O^{ISQ})_2]$. This is not the case for the square-planar cobalt complexes **1**, **4**, and $[Co(^1L_N)_2]$ (Figure 1) for which the observed C–N, C–O, and C–C distances are in better agreement with values of the arithmetic mean between those of an aromatic dianion and the corresponding π-radical monoanion (Scheme 3). Since the two ligands in the neutral molecules are crystallographically identical and no indication for static disorder has been detected, it appears that the unpaired electron is delocalized over both ligands. We propose the following charge distributions: $[Co^{III}(^1L_N^{ISQ})(^1L_N^{IP})]$for $[Co(^1L_N)_2]$, $[Co^{III}(^2L_N^{ISQ})(^2L_N^{IP})]$ for **1**, and $[Co^{III}(^4L_O^{ISQ})(^4L_O^{IP})]$ for **4**. The observed C–O, C–N, and C–C distances in these compounds closely resemble those which were calculated from the arithmetic mean of one mono- and one dianion.

Complex **5** contains the cobaltocenium cation and the $[Co(^4L_O)_2]^-$ ion shown in Figure 7. The overall geometrical features of the monoanion in crystals of **5** are similar to those of the neutral species in crystals of **4**; both are square planar species. As shown in Figure 7 the C–N, and C–O bond lengths in the monoanion of **5** are slightly longer than those in the neutral species in **4** (Figure 6). The C–C bond lengths of the aminophenol ring in **5** and **4** differ also significantly. In complex **5**, six C–C bonds are equidistant within experimental error at $1.40 \pm 0.01$ Å; this clearly indicates the presence of two aromatic, closed-shell, dianionic $(^4L_O^{IP})^{2-}$ ligands. In **4** these six C–C distances show quinoid-type distortions with two alternating shorter C–C bonds. Without any ambiguity the oxidation level of the ligands in **5** are therefore aromatic dianions; this renders the oxidation state

Table 2. Selected bond lengths [Å].

| | | | | | | | |
|---|---|---|---|---|---|---|---|
| Complex **1**[a] | | | | | | | |
| Co–N1 | 1.826(2) | C2–C3 | 1.379(3) | C6–N7 | 1.376(2) | C9–C10 | 1.391(3) |
| Co–N7 | 1.855(2) | C3–C4 | 1.406(3) | N7–C8 | 1.431(2) | C10–C11 | 1.390(3) |
| N1–C1 | 1.354(2) | C4–C5 | 1.379(3) | C8–C13 | 1.392(3) | C11–C12 | 1.387(3) |
| C1–C2 | 1.411(2) | C5–C6 | 1.408(2) | C8–C9 | 1.396(2) | C12–C13 | 1.393(3) |
| C1–C6 | 1.424(2) | | | | | | |
| Complex **2** | | | | | | | |
| Co–N41 | 2.076(4) | C1–C2 | 1.415(7) | C6–N7 | 1.357(6) | C23–C22 | 1.365(7) |
| Co–N1 | 1.864(3) | C2–C3 | 1.370(9) | N7–C8 | 1.424(6) | C21–C22 | 1.410(7) |
| Co–N7 | 1.898(4) | C3–C4 | 1.395(10) | N27–C26 | 1.358(6) | C21–C26 | 1.437(7) |
| Co–N27 | 1.891(4) | C4–C5 | 1.377(9) | C25–C26 | 1.402(7) | C21–N21 | 1.344(6) |
| Co–N21 | 1.866(4) | C5–C6 | 1.411(8) | C24–C25 | 1.385(8) | | |
| N1–C1 | 1.339(6) | C1–C6 | 1.434(7) | C24–C23 | 1.398(8) | | |
| Complex **2a** | | | | | | | |
| Co–N1 | 1.845(2) | C1–C2 | 1.429(4) | C6–N7 | 1.345(3) | C23–C24 | 1.420(4) |
| Co–N21 | 1.853(2) | C1–C6 | 1.443(4) | N7–C8 | 1.447(3) | C24–C25 | 1.370(4) |
| Co–N7 | 1.934(2) | C2–C3 | 1.357(4) | N21–C21 | 1.318(4) | C25–C26 | 1.428(4) |
| Co–N27 | 1.940(2) | C3–C4 | 1.434(4) | C21–C22 | 1.431(4) | C26–N27 | 1.342(4) |
| Co–N40 | 1.989(2) | C4–C5 | 1.364(4) | C21–C26 | 1.452(4) | N27–C28 | 1.442(4) |
| N1–C1 | 1.323(3) | C5–C6 | 1.421(4) | C22–C23 | 1.367(4) | | |
| Complex **3** | | | | | | | |
| Co–I | 2.5745(4) | C2–C3 | 1.362(4) | C8–C9 | 1.388(5) | C21–C26 | 1.440(4) |
| Co–N1 | 1.856(2) | C3–C4 | 1.418(4) | C9–C10 | 1.382(5) | C22–C23 | 1.362(4) |
| Co–N21 | 1.860(2) | C4–C5 | 1.365(4) | C10–C11 | 1.385(6) | C23–C24 | 1.421(5) |
| Co–N7 | 1.882(3) | C5–C6 | 1.417(4) | C11–C12 | 1.379(6) | C24–C25 | 1.370(4) |
| Co–N27 | 1.887(2) | C6–N7 | 1.347(4) | C12–C13 | 1.397(5) | C25–C26 | 1.414(4) |
| N–C1 | 1.328(4) | N7–C8 | 1.434(4) | N21–C21 | 1.329(4) | C26–N27 | 1.338(4) |
| C1–C2 | 1.420(4) | C8–C13 | 1.381(5) | C21–C22 | 1.422(4) | N27–C28 | 1.432(4) |
| C1–C6 | 1.433(4) | | | | | | |
| Complex **4**[a] | | | | | | | |
| Co–O1 | 1.822(2) | C1–C6 | 1.424(4) | N7–C8 | 1.434(3) | C29–C30 | 1.378(4) |
| Co–O26 | 1.823(2) | C2–C3 | 1.384(4) | O26–C26 | 1.327(3) | C30–C31 | 1.411(4) |
| Co–N7 | 1.832(2) | C3–C4 | 1.420(4) | C26–C27 | 1.419(4) | C31–N32 | 1.374(3) |
| Co–N32 | 1.840(2) | C4–C5 | 1.382(4) | C26–C31 | 1.420(4) | N32–C33 | 1.432(3) |
| O1–C1 | 1.329(3) | C5–C6 | 1.402(4) | C27–C28 | 1.387(4) | | |
| C1–C2 | 1.415(4) | C6–N7 | 1.373(3) | C28–C29 | 1.420(4) | | |
| Complex **5**[a] | | | | | | | |
| Co–O1 | 1.830(2) | C1–C6 | 1.402(4) | C3–C4 | 1.397(4) | C6–N7 | 1.388(4) |
| Co–N7 | 1.837(3) | C1–C2 | 1.404(4) | C4–C5 | 1.394(4) | N7–C8 | 1.413(4) |
| O1–C1 | 1.339(3) | C2–C3 | 1.402(4) | C5–C6 | 1.393(4) | | |
| Complex **7**[b] | | | | | | | |
| Co–O1 | 1.845(3) | C2–C3 | 1.367(6) | C9–C10 | 1.385(6) | C33–C34 | 1.430(6) |
| Co–N7 | 1.854(3) | C3–C4 | 1.431(6) | C10–C11 | 1.383(7) | C34–C35 | 1.368(6) |
| Co–O31 | 1.855(3) | C4–C5 | 1.364(6) | C11–C12 | 1.382(7) | C36–N37 | 1.346(5) |
| Co–N37 | 1.859(3) | C5–C6 | 1.410(6) | C12–C13 | 1.381(6) | N37–C38 | 1.422(5) |
| Co–C60 | 2.004(5) | C6–N7 | 1.358(5) | O31–C31 | 1.305(5) | C60–C61 | 1.446(7) |
| O1–C1 | 1.305(5) | N7–C8 | 1.441(5) | C31–C36 | 1.429(6) | C61–N62 | 1.136(6) |
| C1–C6 | 1.419(6) | C8–C13 | 1.384(6) | C31–C32 | 1.430(6) | | |
| C1–C2 | 1.428(6) | C8–C9 | 1.394(6) | C32–C33 | 1.372(6) | | |
| Complex **8** | | | | | | | |
| Ni–O1 | 1.8365(9) | C2–C3 | 1.425(2) | C4–C5 | 1.430(2) | C7–N8 | 1.355(2) |
| Ni–N8 | 1.844(1) | C2–C7 | 1.432(2) | C5–C6 | 1.376(2) | N8–C9 | 1.428(2) |
| O1–C2 | 1.315(2) | C3–C4 | 1.385(2) | C6–C7 | 1.418(2) | | |
| Complex **9** | | | | | | | |
| Ni–N38 | 1.831(3) | C2–C3 | 1.428(5) | N8–C9 | 1.421(5) | C35–C36 | 1.401(6) |
| Ni–N8 | 1.843(3) | C3–C4 | 1.384(6) | O31–C32 | 1.345(5) | C36–C37 | 1.394(6) |
| Ni–O1 | 1.844(2) | C4–C5 | 1.407(6) | C32–C33 | 1.403(6) | C37–N38 | 1.382(5) |
| Ni–O31 | 1.846(3) | C5–C6 | 1.386(6) | C32–C37 | 1.422(6) | N38–C39 | 1.429(5) |
| O1–C2 | 1.329(5) | C6–C7 | 1.410(6) | C33–C34 | 1.411(6) | | |
| C2–C7 | 1.407(6) | C7–N8 | 1.378(5) | C34–C35 | 1.386(6) | | |

[a] Data for one crystallographically independent molecule is given only. [b] Angle: Co-C60-C61: 112.7(3)°.

of the central cobalt ion +III. It is interesting to note that the ligand dimensions in **5** are identical to those observed for diamagnetic, square-planar $[Pd^{II}(bpy)(^3L_O^{IP})]^0$.[14] The charge distribution in the monoanion of **5** is best formulated as $[Co^{III}(^4L_O^{IP})_2]^-$. It is also worth noting that the average Co–N, and Co–O bond lengths in **4** and **5** are 1.835, 1.822 Å and 1.837, 1.830 Å, respectively, and are identical within experimental error of $\pm 0.006$ Å ($3\sigma$). The reduction of the

  

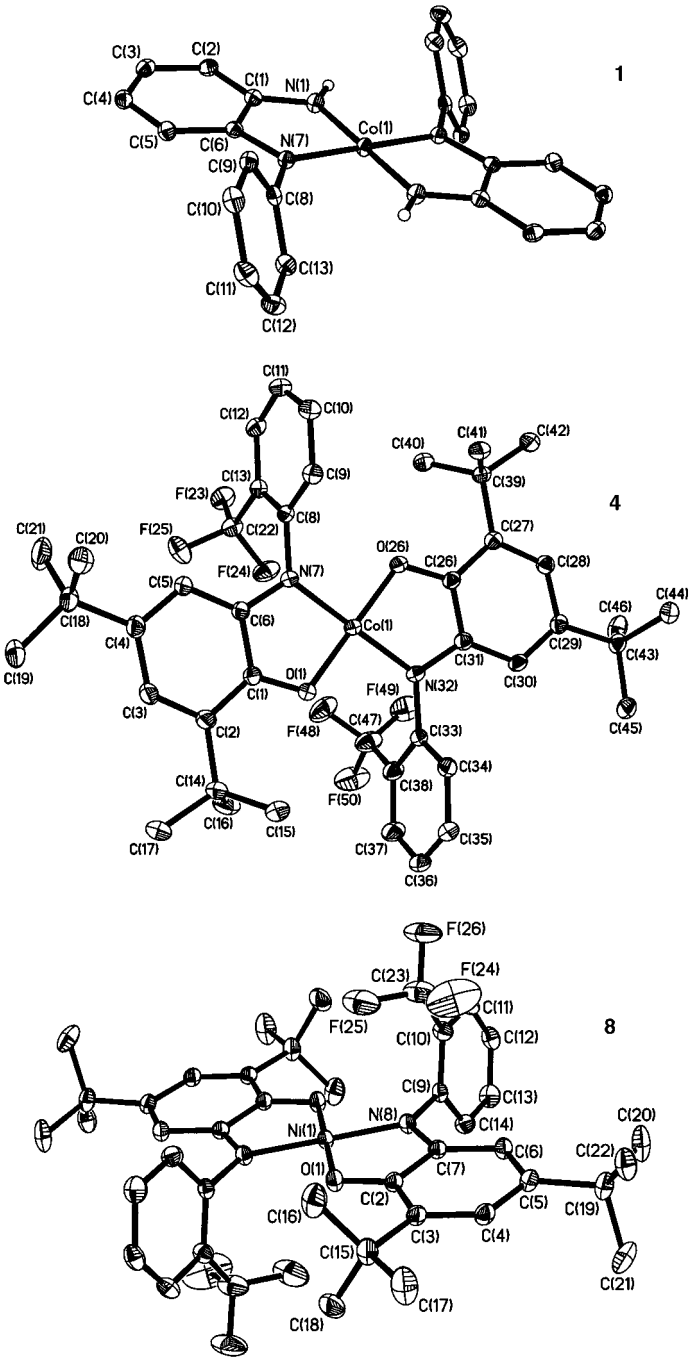


Figure 5. Structure of one of the crystallographically independent molecules of $[Co(^2L_N)_2]^0$ in crystals of **1** (top) and of $[Co(^4L_O)_2]$ in crystals of **4** (middle), and of $[Ni^{II}(^4L)_2]$ in crystals of **8** (bottom).

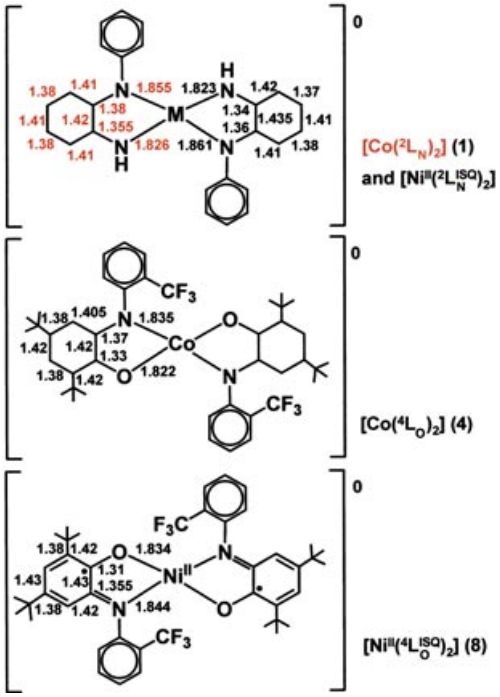


Figure 6. Average C–O, C–N, and C–C distances in Å of the neutral molecules in **1** (in red) and in $[Ni(^2L)_2]$ reference [9a] (in black). Values for complex **4** (middle) and **8** (bottom) are also given. The average experimental error (3σ) is ~±0.01 Å.

neutral species in **4** yielding **5** is therefore unlikely to be a metal-centered process involving $Co^{III} + e^- \rightarrow Co^{II}$.

In the following we describe the structures of the five-coordinate species **2**, **2a**, **3**, and **7** which are shown in Figures 8–10. Average C–N, C–O, and C–C bond lengths of the ligands are given in Figure 8 for **2** and **2a**, Figure 2 for **3**, and Figure 10 for **7**.

In each case the cobalt ion is in a square-base pyramidal environment composed of two bidentate N,N- or N,O-coordinated organic ligands $(L_N)^{n-}$ or $(L_O)^{n-}$ in basal positions and a single halide ion or pyridine as the fifth ligand in the apical position. As mentioned earlier, diamagnetic complexes of this type have been structurally characterized previously: $[Co^{III}(^1L_N^{ISQ})_2Cl]$,[3] *cis*-$[Co^{III}(^2L_N^{ISQ})_2(py)]CH_3CO_2 \cdot H_2O$,[11] $[Co^{III}(^1L_N^{ISQ})_2(PPh_3)]PF_6$,[7] $[Co^{III}(^1L_N^{ISQ})_2(py)]Cl$,[8] and $[Co^{III}(^3L_O^{ISQ})_2X]$ (X = Cl, I).[10] In all of these cases the C–N, C–O, and C–C bond lengths unambiguously indicate that the bidentate ligands possess a benzosemiquinonate(1–) π-radical oxidation level and, consequently, the central cobalt ion invariably possess a +III ($d^6$, low spin, $S_{Co} = 0$) spectroscopic oxidation state.

The structure of the neutral, paramagnetic species *trans*-$[Co(^2L_N)_2(t\text{Bu-py})]$ (**2**) is therefore of great interest, because a different charge distribution must prevail, while the coordination polyhedron remains square-base pyramidal. The charge distribution is either *trans*-$[Co^{III}(^2L_N^{ISQ})(^2L_N^{IP})(t\text{Bu-py})]$ containing a diamagnetic $Co^{III}$ ion ($d^6$, low spin), a paramagnetic benzosemiquinonate(1–) π-radical $(^2L_N^{ISQ})^{\bullet -}$, and a diamagnetic $(^2L_N^{IP})^{2-}$ ion, or, alternatively, *trans*-$[Co^{II}(^2L_N^{ISQ})_2(t\text{Bu-py})]$ containing a low-spin cobalt(II) ion ($d^7$, $S_{Co} = {}^1/_2$) and two antiferromagnetically coupled benzosemiquinonate π radicals $(^2L_N^{ISQ})^{\bullet -}$. The C–N and C–C bond lengths in **2** (Figure 8) indicate that the former description is more appropriate than the latter, because the ligand dimensions resemble those of an averaged mono- and dianion, $(^2L_N^{ISQ})^{\bullet -}$ and $(^2L_N^{IP})^{2-}$. In contrast, these bonds in diamagnetic *cis*-

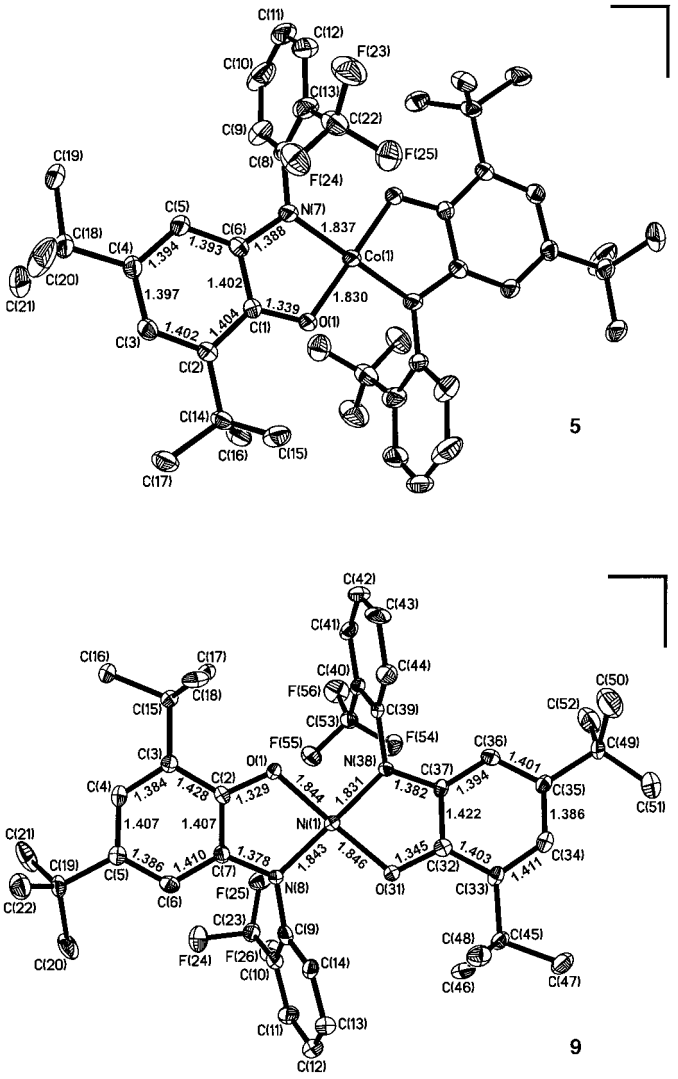


Figure 7. Structures of the monoanions $[Co^{III}(^4L)_2]^-$ in crystals of **5** (top) and $[Ni^{II}(^4L)(^4L)]^-$ in crystals of **9** (bottom). The error of the C–N, C–O, and C–C bond lengths is ±0.01 Å (3σ) for **5** and ±0.015 Å for **9**.

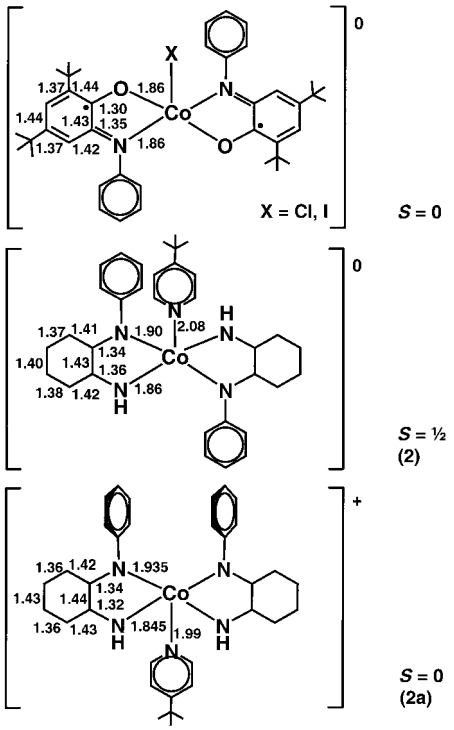


Figure 8. Average C–N, C–O, and C–C distances [Å] in a diamagnetic neutral molecule of $[Co^{III}(^4L)_2X]$ (X = Cl, I) from reference [10] and $[Co(^2L_N)_2(t\text{Bu-py})]$ in crystals of **2** (middle) and *cis*-$[Co(^2L_N)_2(t\text{Bu-py})]^+$ in **2a** (bottom).

$[Co^{II}(^2L_N^{ISQ})_2(py)]^+$[11] are in excellent agreement with the presence of two $(^2L_N^{ISQ})^{\bullet-}$ π radicals. They are the same as in $[Co^{III}(^2L_N^{ISQ})_2I]$ (**3**) (Figure 2).

The structure of the neutral complex in crystals of **7** clearly indicates the presence of two ligand π radicals $(^4L_O^{ISQ})^{\bullet-}$ and the C-coordinated monoanion of acetonitrile, $(CH_2CN)^-$, in the apical position (Figures 9 and 10). The geometrical features of the benzosemiquinonate(1−) radicals are, within experimental error, identical with those reported previously for $[Co^{III}(^3L_O^{ISQ})X]$ (X = Cl, I).[10] A few complexes containing C-coordinated $(CH_2CN)^-$ ions have been structurally characterized.[33] The C–N, C–O, and C–C bond lengths of the $(^4L_O^{ISQ})^{1-}$ ligands found here in five-coordinate **7** are also identical to those reported in octahedral $[Co^{III}(^3L_O^{ISQ})_3]$ with an $S = {}^2/_3$ ground state.[15]

The nickel complex **8** contains square-planar, diamagnetic, neutral $[Ni^{II}(^4L_O^{ISQ})_2]$ molecules (Figures 5 and 6). The C–O, C–N, and C–C bond lengths clearly show the presence of two $(^4L_O^{ISQ})^{\bullet-}$ π radicals. As shown in Figure 6 these bond lengths differ slightly from those in the cobalt complex **4**; this indicates that the respective ligand oxidation levels in both species differ (and, concomitantly, the metal oxidation states) and we assign them as $[Ni^{II}(^4L_O^{ISQ})_2]$ in **8** and $[Co^{III}(^4L_O^{ISQ})(L_O^{IP})]$ in **4.**

Similarly, the C–O, C–N, and C–C bond lengths in the structures of the monoanions in crystals of **5** and **9** shown in Figure 7 differ slightly. Both are square-planar species, but the dimensions of the ligands indicate the presence of two o-iminophenolate(2−) dianions in **5** as shown above, whereas in **9** the C–O, C–N, and C–C distances are more in agreement with the average between one *o*-iminobenzosemiquinonate(1−) and an *o*-iminophenolate(2−) and a central nickel(II) ion: $[Ni^{II}(^4L_O^{ISQ})(^4L_O^{IP})]^-$.

It is also interesting to note that the corresponding M–O and M–N bond lengths of the neutral complexes **4** and **8** are slightly shorter in the cobalt complex **4**. The same is true for the monoanions in **5** and **9**, in which these bonds are also shorter in the cobalt complex **5**. If both metal ions possess the same oxidation state +II, we would expect that the low-spin $Co^{II}$–X bond lengths to be longer than those of the corresponding $Ni^{II}$–X bonds.

**Electro- and spectroelectrochemistry**: Cyclic voltammograms (CV) of complexes **1**, **4**, and **8** were recorded in $CH_2Cl_2$ containing 0.10 M $[n\text{Bu}_4\text{N}]PF_6$ as a supporting electrolyte at a glassy carbon working electrode and an Ag/

  

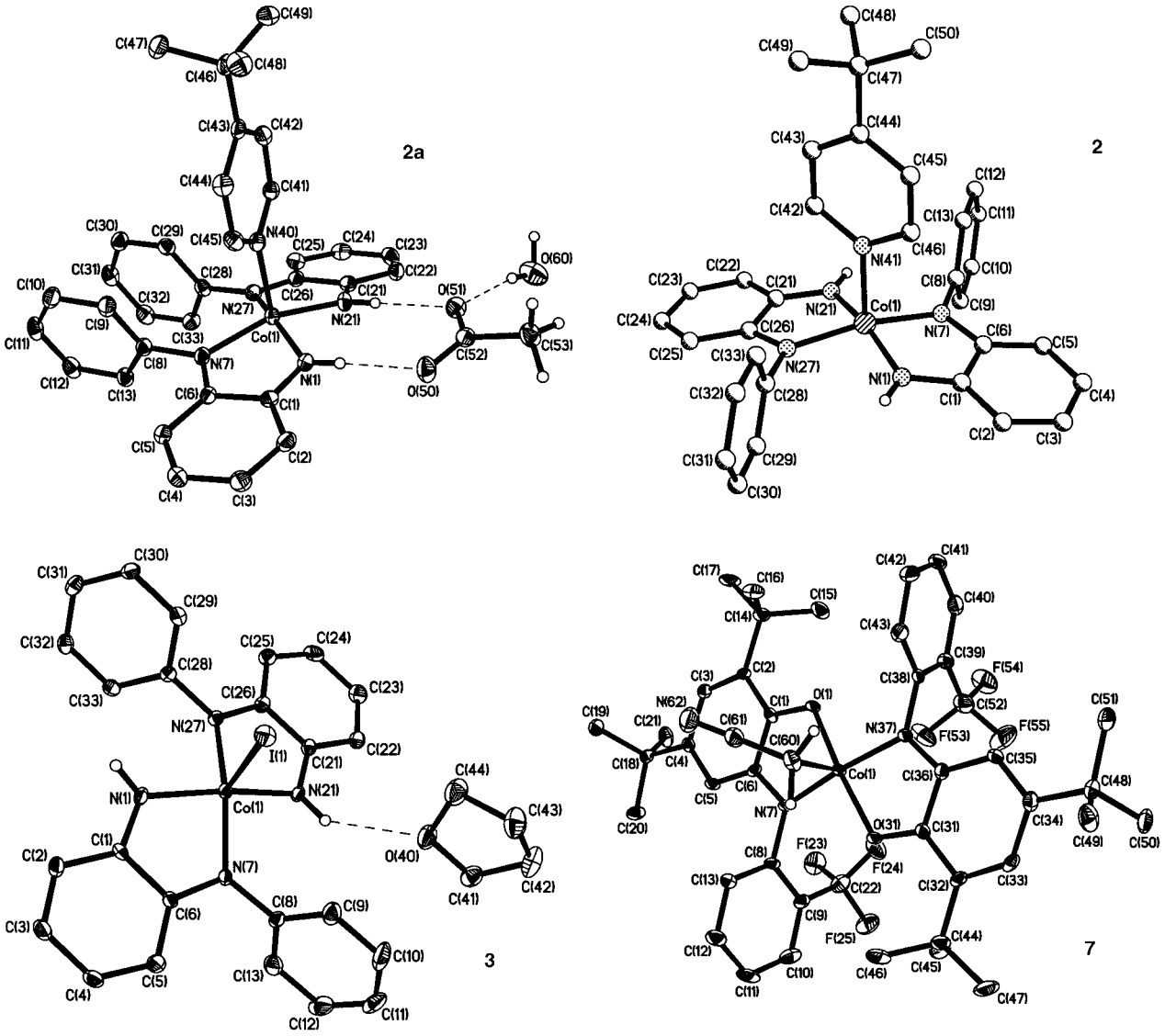


Figure 9. Structures of the ion pair in crystals of **2a** and of the neutral complexes in crystals of **2**, **3**, and **7**.

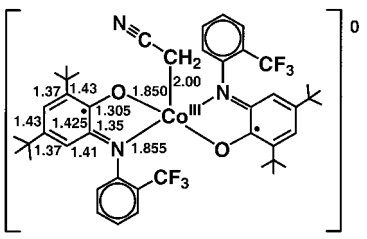


Figure 10. Bond lengths [Å] of the neutral complex $[Co^{III}(^4L)_2(CH_2CN)]$ in crystals of **7**. Experimental error: ±0.02 Å (3σ).

Table 3. Redox potentials of complexes versus $Fc^+/Fc$.[a]

| | $E^1_{1/2}$ [V] $+1 \rightleftharpoons 0$ | $E^2_{1/2}$ [V] $0 \rightleftharpoons -1$ | $E^3_{1/2}$ [V] $-1 \rightleftharpoons -2$ |
|---|---|---|---|
| $[Co(^1L_N)_2]$[b] | −0.32 | −0.95 | −1.98 |
| **1** | −0.50 | −1.03 | |
| **4** | −0.20 | −0.85 | |
| **8** | +0.04(2e) | −1.01 | −1.74 |

[a] Conditions: glassy carbon working electrode, $Ag/AgNO_3$ reference electrode; 20 °C; $CH_2Cl_2$ containing 0.10 M $[(n\text{Bu})_4N]PF_6$ supporting electrolyte; [complex] ~ $10^{-3}$ M: scan rate 100 mV $s^{-1}$. [b] Reference [1].

$AgNO_3$ reference electrode. Ferrocene was used as an internal standard; all potentials are referenced versus the ferrocenium/ferrocene couple ($Fc^+/Fc$). Table 3 summarizes the results.

The CV of **1** displays two reversible one-electron transfer waves in the potential range −1.5 to 0.0 V; a reversible one-electron oxidation at $E^1_{1/2} = -0.50$ V and a reversible one-electron reduction at $E^2_{1/2} = -1.03$ V. Similar waves have been reorted by Balch and Holm[1] for $[Co(^1L_N)_2]$; they report a second one-electron reduction at $E^3_{1/2} = -1.98$ V for the mono-/dianion couple.

The CV of **4** is very similar; again a reversible one-electron oxidation ($E^1_{1/2} = -0.20$ V) and a reversible one-electron

reduction ($E^2_{1/2} = -0.85$ V) are observed. Since we have structurally characterized the neutral species **4** and its monoanion in **5** and shown that both contain a cobalt(III) ion, we assign the charge distribution as shown in Equations (2) and (3).

$$[Co(^2L_N)_2]^+ \underset{+e}{\overset{-e}{\rightleftharpoons}} [Co^{III}(^2L_N^{ISQ})(^2L_N^{IP})]^0 \underset{+e}{\overset{-e}{\rightleftharpoons}} [Co^{III}(^2L_N^{IP})_2]^- \quad (2)$$

$$[Co(^4L_O)_2]^+ \underset{+e}{\overset{-e}{\rightleftharpoons}} [Co^{III}(^4L_O^{ISQ})(^4L_O^{IP})]^0 \underset{+e}{\overset{-e}{\rightleftharpoons}} [Co^{III}(^4L_O^{IP})_2]^- \quad (3)$$

The oxidized and reduced species of **1** and **4** are stable in solution on the timescale of a coulometric experiment. Therefore, it has been possible to record the electronic spectra of the monocations of the neutral species **1** and **4**, and of their corresponding monoanions. The results are shown in Figure 11 and summarized in Table 4. From the crystal structure of **5**, which contains the square-planar, paramagnetic ion $[Co^{III}(^4L_O^{IP})_2]^-$, we conclude that the electrochemically generated ion $[Co^{III}(^2L_N^{IP})_2]^-$ is also square-planar and paramagnetic ($S=1$). The four-coordinate monocations have not yet been isolated as salts or structurally characterized; only the five-coordinate species **2**, **2a**, **3**, and **7** are synthetically accessible.

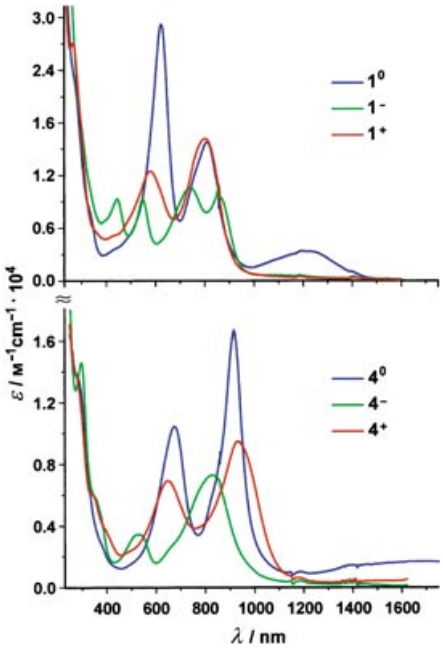


Figure 11. Electronic spectra of **1** and its electrochemically generated monoanion and monocation (top), respectively, in $CH_3CN$ solution (0.10 M $[(n\text{Bu})_4\text{N}]PF_6$) and, correspondingly, those of **4**, **4**$^-$, and **4**$^+$ (bottom).

The CV of **8** is very similar to that reported for $[Ni^{II}(^3L_O^{ISQ})_2]$.[12] Two successive one-electron reductions of **8** in $CH_2Cl_2$ (0.10 M $[(n\text{-Bu})_4\text{N}]PF_6$) are observed at $-1.01$ and $-1.74$ V. These processes have been assigned as ligand-centered processes as in Equation (4).

Table 4. Electronic spectra of complexes.

| | Solvent | $\lambda_{max}$ [nm] ($10^4$ $\varepsilon$ [M$^{-1}$cm$^{-1}$]) |
|---|---|---|
| **1** | $CH_3CN$ | 360 sh(0.85), 625(3.0), 816(1.5), 1230(0.40) |
| **1**$^-$ | $CH_3CN$[a] | 445(0.9), 530(0.9), 740(1.0), 870(0.80) |
| **1**$^+$ | $CH_3CN$[a] | 350 sh(2.6), 580(1.2), 800(1.5) |
| **2** | $CH_2Cl_2$ | 324 sh(0.8), 628(2.5), 819(1.3), 1230(0.3) |
| **2a** | $CH_2Cl_2$ | 280(1.9), 463(0.4), 594(1.6), 786(1.3) |
| **3** | $CH_2Cl_2$ | 269(3.2), 397(0.8), 436(0.85), 514(1.2), 636(2.6), 786(1.9) |
| **4** | $CH_2Cl_2$ | 300 sh(2.0), 676(1.6), 916(2.5), 1600(0.25) |
| **4**$^-$ (**5**) | $CH_2Cl_2$[a] | 400 sh(0.6), 535(0.35), 720 sh(0.33), 827(0.7) |
| **4**$^+$ | $CH_2Cl_2$[a] | 300 sh(1.28), 350 sh(0.5), 620(0.7), 960(1.1) |
| **7** | $CH_3CN$ | 280(0.3), 440 sh, 505(0.9), 629(0.34), 831(0.35) |
| **8** | $CH_2Cl_2$ | 350(3.0), 600(0.2), 900(1.6) |
| **9** | $CH_2Cl_2$ | 382 sh, 608(0.1), 885(0.3), 1340(1.0) |
| $[Co(^1L_N)_2]$[b] | DMF, DMSO | 337(0.5), 420(0.3), 588(1.9), 763(1.2), 1135(0.4) |
| $[Co(^1L_N)_2]I$[c] | DMF | 260(1.1), 410(0.2), 490(0.4), 607(1.6), 751(0.8) |

[a] Electrochemically generated in solutions containing 0.10 M $[(n\text{Bu})_4\text{N}]PF_6$ supporting electrolyte; [b] Reference [1]. [c] Reference [15].

$$[Ni^{II}(^4L_O^{ISQ})_2] \underset{+e}{\overset{-e}{\rightleftharpoons}} [Ni^{II}(^4L_O^{ISQ})(^4L_O^{IP})]^- \underset{+e}{\overset{-e}{\rightleftharpoons}} [Ni^{II}(^4L_O^{IP})_2]^{2-} \quad (4)$$

Controlled-potential coulometry at $+0.6$ V shows that **8** can be oxidized in a nearly reversible one-step, two-electron oxidation yielding the $[Ni^{II}(^4L_O^{IBQ})_2]^{2+}$ ion.

**X-band EPR spectra**: The X-band EPR spectra of four-coordinate **1** at 10 K in $CH_2Cl_2$/toluene (1:1 v/v) and of five-coordinate **2** in 4-*tert*-butylpyridine/toluene at 10 K shown in Figure 12 confirm the $S=\frac{1}{2}$ ground state of both species.

The spectrum of **1** has been successfully simulated by using the following parameters: $g_x = 1.9906$, $g_y = 2.0508$, $g_z =$

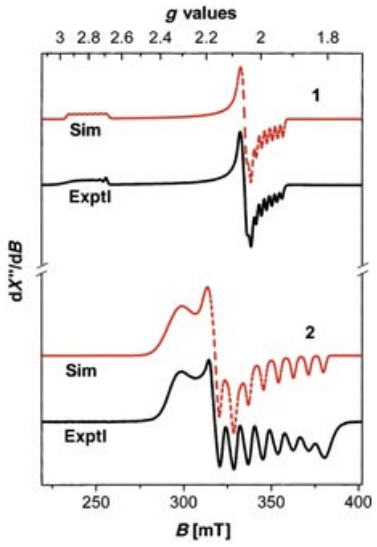


Figure 12. X-band EPR spectra of **1** (top) and **2** (bottom). Conditions for **1**: $CH_3CN$ at 30 K; frequency 9.6351 GHz; power 505.3 μW; modulation amplitude 10 G. Conditions for **2**: 4-*tert*-butylpyridine/toluene mixture (1:3) at 10 K; frequency 9.6345 GHz; power 20 μW; modulation amplitude 10 G.

  

2.8100 ($g_{iso}=2.3140$) with $^{59}$Co hyperfine coupling constants $A_{xx}=24.0$, $A_{yy}=0$, $A_{zz}=42$ G (line width $W_x=20$ G, $W_y=37$ G, $W_z=38$ G). The spectrum indicates that the unpaired electron resides in a metal d orbital; it resembles closely those reported for many square-planar $Co^{II}$ (low spin $d^7$) complexes.[6] On the other hand, a cobalt(III) ion in a square-planar ligand field possesses an $S_{Co}=1$ local spin state;[31,32] strong antiferromagnetic coupling then yields an $S=1/2$ ground state again with an unpaired electron in the same metal d orbital as above. Thus, it is not straightforwardly possible to discern between **A** and **B** in Scheme 2 by EPR spectroscopy.

The rhombic signal of five-coordinate **2** has been satisfactorily modeled by using the following parameters: $g_x=1.9694$, $g_y=2.1275$, $g_z=2.3100$ ($g_{iso}=2.1402$) with $^{59}$Co hyperfine coupling constants $A_{xx}=84.8$, $A_{yy}=15.1$, $A_{zz}=0$ G ($W_x=34.7$, $W_y=76.0$, $W_z=190$ G).

The rhombic X-band EPR spectrum of **4** in frozen $CH_2Cl_2$ solution at 90 K is very similar to that of **1**: $g_x=1.97$, $g_y=2.03$, $g_z=3.11$ ($g_{iso}=2.43$). The $S=1/2$ signal displays no resolvable $^{59}$Co hyperfine splitting.

The X-band EPR spectrum of **9** in frozen $CH_2Cl_2$ at 90 K exhibits a rhombic signal ($g_x=2.075$, $g_y=2.014$, $g_z=2.046$ ($g_{iso}=2.045$)), which resembles closely those reported for many square-planar bis(dioxolene)nickel(II) monoanions with an $S=1/2$ ground state.[9] These spectra have recently been interpreted[9] in terms of a central, diamagnetic nickel(II) ion ($d^8$), a $(L_O^{IP})^{2-}$ ion and a π-radical ion $(L_O^{ISQ})^{\bullet-}$, in which the unpaired electron is delocalized over both ligands. The SOMO of these compounds, $b_{2g}$ under $D_{2h}$ symmetry, is basically the antisymmetric combination of the SOMO of the free semiquinonate(1−) ligand; it transforms "gerade" under inversion and, therefore, mixes with the out-of-plane $d_{xz}$ orbital of the nickel(II) and thereby acquires some metal d character (~15%), which in turn gives rise to a sizeable nickel hyperfine coupling. Since the ground state $^2B_{2g}$ readily mixes with relatively low-lying d–d excited states, it has a reasonably large orbital angular momentum that manifests itself in a relatively large $g$ anisotropy.[9,14] The charge distribution in the monoanion **9** is therefore correctly described by the two resonance structures: $[Ni^{II}(^4L_O^{IP})(^4L_O^{ISQ})]^- \rightleftarrows [Ni^{II}(^4L_O^{ISQ})(^4L_O^{IP})]^-$.

**Electronic spectra**: The electronic spectra of complexes have been recorded in the range 280–2000 nm in $CH_2Cl_2$ or $CH_3CN$. In some cases the species were generated electrochemically by means of controlled potential coulometry in solutions containing 0.1 M $[N(n\text{-}Bu)_4]PF_6$ as a supporting electrolyte. The results are summarized in Table 4.

Complexes **1**, **2**, **2a**, **3**, **4**, **5**, **7**, **8**, and **9** are all highly colored and display a varying number of intense absorption maxima ($\varepsilon > 5\times10^3$ M$^{-1}$cm$^{-1}$) in the visible and near infrared regions. These absorption maxima do not represent d–d transitions; they are spin-allowed ligand-to-metal (LMCT) or ligand-to-ligand charge-transfer bands (LLCT).

It is instructive to first discuss the spectra of neutral nickel complex **8** and its monoanion **9**, both of which exhibit a single very intense band at 900 nm ($\varepsilon=4.6\times10^4$ M$^{-1}$cm$^{-1}$) and 1340 nm ($1.0\times10^4$ M$^{-1}$cm$^{-1}$), respectively.[12] For comparison, the corresponding complexes $[Ni^{II}(^2L_N^{ISQ})_2]$ and $[Ni^{II}(^2L_N^{ISQ})(^2L_N^{IP})]^-$ display these bands at 839 ($4.0\times10^4$ M$^{-1}$cm$^{-1}$) and at 1119 nm ($1.7\times10^4$ M$^{-1}$cm$^{-1}$),[9] respectively.

For the neutral species $[Ni^{II}(^1L_N^{ISQ})_2]$, it has been established[9] that the upper valence region contains four doubly occupied MOs that are predominantly centered on the central $Ni^{II}$ ion ($d^8$). The LUMO+1 orbital is dominated by the Ni $d_{x^2-y^2}$ MO, which is strongly σ antibonding with the ligands. The HOMO–LUMO transition $1b_{1u}\rightarrow2b_{2g}$ represents the intense LLCT band. No other LMCT bands are observed in the visible region. In the corresponding monoanion the former LUMO ($2b_{2g}$) becomes the SOMO, which has ~15% Ni $3d_{xz}$ character; the transition $1b_{1u}\rightarrow2b_{2g}$ is again electric dipole and spin-allowed and represents a ligand-to-ligand intervalence charge-transfer band (LLIVCT).

Figure 13 exhibits the spectra of **2**, **2a**, and **3**; the similarity of these is quite remarkable. Complexes **1** (Figure 11) and **2** exhibit each a LLCT band at 1230 nm with an intensity of

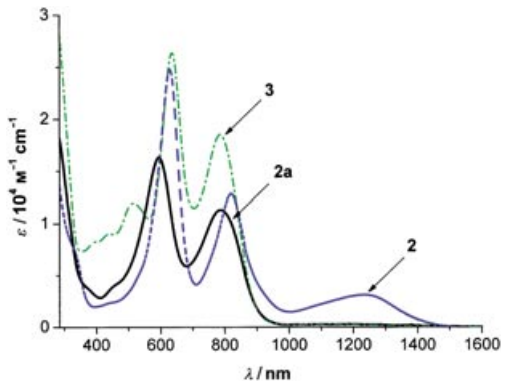


Figure 13. Electronic spectra of **2**, **2a**, and **3** in $CH_2Cl_2$.

~$3\times10^3$ M$^{-1}$cm$^{-1}$. Thus, increasing the coordination number from four to five on going from **1** to **2** does not influence the electronic spectrum greatly. In fact, the spectral differences between **1** and **2** in solution are so small that the solid-state spectra of both species were also recorded and confirmed their similarity. In contrast, the spectra of five-coordinate **2a** and its formally one-electron oxidized analogue **3** (Figure 13) and, similarly, that of **7** do not display an intense absorption maximum >900 nm. Instead, two intense maxima at ~800 and ~600 nm are observed that are assigned LMCT bands.

Interestingly, the spectrum of the electrochemically generated four-coordinate monoanion of **1** in $CH_3CN$ exhibits four intense (~$3\times10^3$ M$^{-1}$cm$^{-1}$) LMCT bands at 445, 530, 740 and 870 nm.

The spectrum of square-planar **4** shown in Figure 11 is very similar to that of **1**: a band at 1600 nm ($2.5\times10^3$ M$^{-1}$cm$^{-1}$), two intense LMCT maxima at 916 and 676 nm, and a shoulder at ~300 nm are observed. The spec-

trum of the monoanion in **5** is interesting; it displays two intense maxima at 827 and 535 nm and two shoulders at 720 and ~390 nm.

## Calculations

*Bonding schemes*: As shown in Table 5 the optimized calculated structures of $[M(^1L_N)_2]^{0,1-}$ (M = Co, Ni) are in excellent agreement with the experimental findings. The slight overestimation of the Co–N and Ni–N distances is typical of present day DFT functionals. However, the metrical parameters for the organic ligands are very accurately reproduced by the calculations with the typical error in computed bond lengths not exceeding ~0.02 Å.

Table 5. Calculated and experimental (in parentheses) bond lengths [Å] in $[Co(^1L_N)_2]$, $[Co(^1L_N)_2]^-$, and $[Ni(^1L_N)_2]$, $[Ni(^1L)_2]^-$.

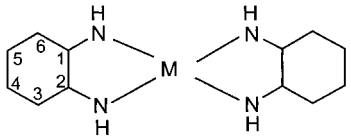


| | $[Co(^1L_N)_2]$[a] | $[Co(^1L_N)_2]^-$[b] | $[Ni(^1L)_2]$[c] | $[Ni(^1L_N)_2]^-$[c] |
|---|---|---|---|---|
| M–N | 1.841 (1.841(2)) | 1.866 (1.833(3)) | 1.841 (1.822) | 1.857 (1.843(3)) |
| C–N | 1.367 (1.365(2)) | 1.377 (1.369(4)) | 1.350 (1.350) | 1.361 (1.378(5)) |
| C1–C2 | 1.446 (1.424(2)) | 1.438 (1.417(4)) | 1.446 (1.429) | 1.427 (1.407(6)) |
| C2–C3 | 1.417 (1.408(2)) | 1.411 (1.391(4)) | 1.416 (1.425) | 1.410 (1.410(6)) |
| C3–C4 | 1.399 (1.379(3)) | 1.415 (1.398(4)) | 1.386 (1.383) | 1.403 (1.389(6)) |
| C4–C5 | 1.419 (1.406(3)) | 1.406 (1.401(4)) | 1.421 (1.423) | 1.407 (1.405(6)) |

[a] From this work for **1**. [b] From this work for **5**. [c] From reference [9a,b] for $[Ni(^1L)_2]$ in which the ligand has two tertiary butyl groups at C3 and C5.

For the MO description of the complexes $[Co(^1L_N)_2]^{0,1-}$ within the $D_{2h}$ point group we choose the $z$ axis to be along the normal of the planar complexes, the $x$ axis along the long axis, and the $y$ axis along the short axis of the complexes as shown in Figure 14. The qualitative bonding scheme derived from the spin-unrestricted B3LYP DFT calculations are also shown in Figure 14, in which the spin-up and spin-down Kohn–Sham MOs are plotted in order of increasing energy. Since the MO scheme qualitatively does not change on going from the neutral $[Co(^1L_N)_2]$ species to its one-electron reduced monoanionic form, it is only given for $[Co(^1L_N)_2]^{1-}$. The compositions of selected orbitals are summarized in Table 6. We will argue below that the description of neutral $[Co(^1L_N)_2]^0$ complex in terms of a single configuration is slightly oversimplified, but for all practical purposes of this section the single-determinant description is adequate. The ground-state electronic configuration of $[Co(^1L_N)_2]^{1-}$, as shown in Figure 14, is $(1a_g)^2(2a_g)^2(1b_{3g})^2(1a_u)^2(1b_{2g})^2(1b_{1u})^2(2b_{2g})^1(2b_{3g})^1(1b_{1g})^0$.

The $1b_{1g}$ LUMO of the monoanion represents the antibonding combination of the Co $3d_{xy}$ and the ligand σ orbitals. Due to the ligand geometry the overlap between these two orbitals is very favorable and provides an efficient pathway for the ligand-to-metal electron donation. The $2b_{2g}$ and the $2b_{3g}$ orbitals remain singly occupied yielding a spin-triplet ground state for the monoanion (as is observed). The energy gap between these two SOMOs is found to be too small to stabilize the alternative spin-singlet state as had been suggested for some bis(benzodithiolato)cobalt(III) complexes.[34] The first spin-triplet state is found to be ~10 kcal mol$^{-1}$ (0.43 eV) lower in energy than the corresponding spin singlet state in the B3LYP calculations.

The $2b_{2g}$ orbital is an out-of-plane orbital with almost equal contributions from the Co $3d_{xz}$ and the ligand $b_{2g}$ fragment orbitals (Table 6). The $2b_{3g}$ orbital, on the other hand, is predominantly Co $3d_{yz}$ in character; it undergoes little mixing with the low-lying ligand $b_{3g}$ fragment orbital. The remaining two Co $3d_{x^2-y^2}$ ($1a_g$) and $3d_{z^2}$ ($2a_g$) orbitals do not strongly interact with ligand orbitals and are placed at comparatively lower energies. The d-orbital splitting in $[Co(^1L_N)_2]^{1-}$ is thus $3d_{x^2-y^2}$, $3d_{z^2} < 3d_{xz}$, $3d_{yz} < 3d_{xy}$, which is nicely compatible with ligand-field theory. Analysis of the optical and magnetic data will show that the $3d_{z^2}$ and the $3d_{yz}$ orbitals lie very close to each other in energy.

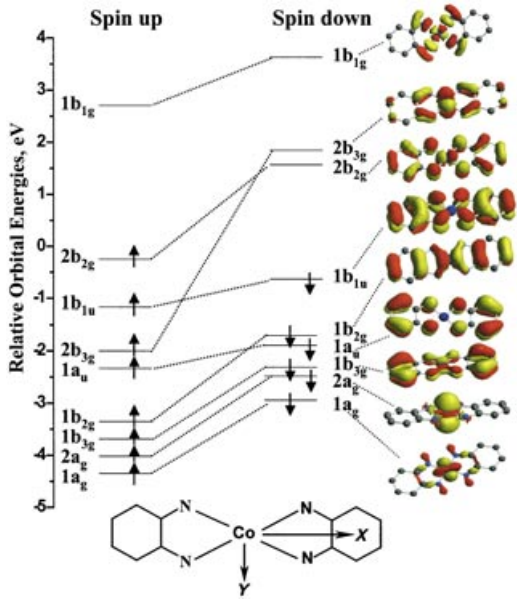


Figure 14. Kohn–Sham MO orbitals and energy scheme of **1** from an spin unrestricted B3LYP DFT calculation.

One-electron oxidation of the monoanion yielding the neutral complex generates an additional hole in the out-of-plane $2b_{2g}$ orbital, which becomes the LUMO of the $[Co(^1L_N)_2]$ species. The calculated ground-state electronic

  

Table 6. Percentage composition of the selected orbitals of $[Co(^1L_N)_2]$ and $[Co(^1L_N)_2]^-$.

| | MO | M($3d_{yz}$) | M($3d_{xz}$) | M($3d_{xy}$) | N($2p_z$) | N($2p_{x,y}$) | C($2p_z$) | C($2p_{x,y}$) |
|---|---|---|---|---|---|---|---|---|
| $[Co(^1L_N)_2]^-$ | $2b_{2g}$ | | 47.1 | | 28 | | 24 | |
| | $2b_{3g}$ | 75 | | | 10 | | 12 | 2 |
| | $1b_{1g}$ | | | 61 | | 24 | | |
| $[Co(^1L_N)_2]$ | $2b_{2g}$ | | 35.2 | | 34.2 | | 28 | |
| | $2b_{3g}$ | 73 | | | 12 | | 14 | |
| | $1b_{1g}$ | | | 61 | | 22 | | 3 |

configuration for this neutral species ($S=1/2$) is then $(1a_g)^2(2a_g)^2(1b_{3g})^2(1a_u)^2(1b_{2g})^2(1b_{1u})^2(2b_{3g})^1(2b_{2g})^0(1b_{1g})^0$.

This oxidation is accompanied by a 12% decrease in the Co $3d_{xz}$ character of the $2b_{2g}$ orbital. However, the compositions of the SOMO ($2b_{3g}$) and of the LUMO+1 ($1b_{1g}$) do not change significantly upon oxidation. The unpaired electron of the neutral species is located in a predominantly metal based $2b_{3g}$ orbital in agreement with the observed large anisotropy of the EPR *g* tensor in **1** (Figure 12).

It is now interesting to compare the electronic structures of **1** and of its monoanion with those reported for the corresponding two nickel complexes, namely $[Ni(^1L_N)_2]$ and $[Ni(^1L_N)_2]^{1-}$, which have in part been studied previously.[9] The frontier orbitals calculated here for the cobalt complexes are very similar to those reported for the nickel species with the notable exception that the $2b_{2g}$ and $2b_{3g}$ orbitals are predominantly ligand-based orbitals in the nickel cases. As can be verified from the data in Table 6, these orbitals are significantly more metal-based in the corresponding two cobalt species. This is consistent with the considerably higher effective nuclear charge of nickel(II) relative to $Co^{II}$. This has been previously shown by X-ray absorption spectra of divalent metal chlorides.[35]

Thus it appears to be justified by the DFT calculations to assign a +II spectroscopic oxidation state to the central nickel ions in *both* complexes, namely in $[Ni(^1L_N)_2]$ and $[Ni(^1L_N)_2]^-$. Thus, for neutral, square-planar $[Ni^{II}(^1L_N^{ISQ})_2]$ a detailed model study as well as high-level electronic structure calculations[9] have shown that the complex is best described as a species that contains two strongly interacting ligand radicals, $(L_N^{ISQ})^{\bullet-}$ coordinated to a diamagnetic central nickel(II) ion ($d^8$). The ligands have been shown to interact with each other through an efficient superexchange mechanism mediated by a back-bonding interaction to the central metal ion yielding a singlet diradical.

From the corresponding DFT calculations for the monoanion $[Ni(^1L_N)_2]^{1-}$, an unambiguous interpretation of the valence state has also been found.[9] The ground-state configuration is in this case $(1a_g)^2(2a_g)^2(1b_{3g})^2(1a_u)^2(1b_{2g})^2(2b_{3g})^2(1b_{1u})^2(2b_{2g})^1(1b_{1g})^0$. The $2b_{2g}$ level is again ligand-centered with some 26% Ni $3d_{xz}$ character.

The redox-active $2b_{2g}$ orbital (LUMO of the neutral species, but SOMO in the anion) is predominantly ligand-based and is associated with a small π interaction with the low-lying Ni $3d_{xz}$ orbital. As pointed out above, the predominance of the ligand character in the $2b_{2g}$ level arises from the higher effective nuclear charge of Ni (relative to Co) which brings the 3d orbitals much lower in energy relative to the ligand orbitals. The upper valence region of the two nickel complexes is therefore composed of four doubly occupied MOs that are predominantly centered on nickel ($d^8$, $Ni^{II}$).

In contrast, for $[Co(^1L_N)_2]^{1-}$ the DFT calculations allow us to envisage two extreme descriptions for its electronic structure (Figure 15): 1) If the $2b_{2g}$ orbital has predominantly

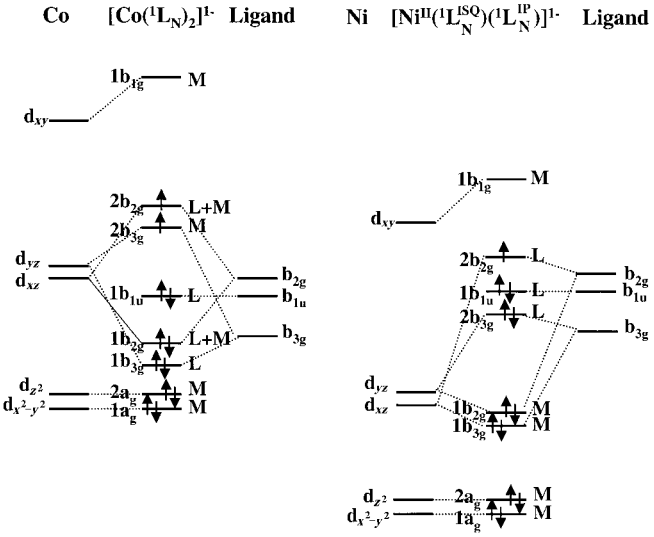


Figure 15. MO schemes of $[Co(^1L_N)_2]^{1-}$ and of $[Ni^{II}(^1L_N^{ISQ})(^1L_N^{IP})]^{1-}$.

metal character (Co), then the anionic complex could be described as a species that contains a $d^6$ configuration with an intermediate spin ($S=1$) cobalt(III) ion; and 2) if, on the other hand, the $2b_{2g}$ orbital possesses pure ligand character, a $Co^{II}$ low-spin $d^7$ configuration with a ferromagnetically coupled $(^1L_N^{ISQ})^{\bullet-}$ ligand π radical would prevail. The actual DFT calculations on $[Co(^1L_N)_2]^{1-}$ reveal that the $2b_{2g}$ orbital has almost equal metal and ligand contributions.

It is therefore not possible to determine an unequivocal $d^n$ ($n=6$ or 7) electron configuration at the metal ion and assign unambiguously a spectroscopic oxidation state of the central cobalt ion. We note that the closed-shell-like ligand configuration $(^4L_O^{IP})^{2-}$ as determined by X-ray crystallography for **5** does point to a more pronounced $Co^{III}$ ($d^6$, $S=1$) spectroscopic oxidation state than a $[Co^{II}(^4L_O^{ISQ})(^4L_O^{IP})]^-$ mixed-valent configuration.

Similarly, for the neutral complex $[Co(^1L_N)_2]$ the metal contribution in the $2b_{2g}$ orbital (the LUMO) is high (35%), and the description of the electronic structure of this neutral species as containing a low-spin $Co^{II}$ ion coordinated to two antiferromagnetically coupled ligand π radicals, $(^1L_N^{ISQ})^{1-}$, is

ambiguous. However, such a description is in somewhat better agreement with the multiconfigurational ab initio calculations presented below. We stress that the question of the spectroscopic (physical) oxidation state of the central cobalt ion may again not be resolvable for the neutral $[Co(^1L_N)_2]$ species in an unambiguous fashion.

*Excited state calculations*: The optical electronic spectra of the corresponding $[M(^1L_N)_2]^n$ complexes of Ni, Pd, and Pt ($n=0,1-$) have been analyzed in some detail previously.[9] It was shown that the very intense absorption in the near-IR region ($\varepsilon > 10^4 L\,mol^{-1}\,cm^{-1}$) of the spectra corresponds to a ligand-to-ligand charge transition (LLCT) that contains considerable information on the diradical character of the neutral species and the ground-state ligand–ligand exchange coupling. In the monoanionic (and monocationic) metal $d^8$ species, this intense absorption band corresponds to an intervalence transition (IVCT) of the type $[LML^{\cdot}]^{1-\text{ or }1+} \rightleftarrows [L^{\cdot}ML]^{1-\text{ or }1+}$, in which $L^{\cdot}$ represents the semiquinonate(1−) π-radical form of the ligand and L denotes the aromatic dianionic form in the monoanion or the neutral quinonane form in the monocation. The position, shape, and intensity of these observed IVCT were clearly indicative of class III mixed-valence systems with complete electron delocalization of the unpaired electron over both ligands.[9]

In the present case of the corresponding cobalt complexes these optical absorption spectra (Figure 11) have a considerably more complicated appearance and, consequently, their analysis is more involved.

The room-temperature absorption and low-temperature MCD (1.8 K, 5 T) spectra of **1** have been subjected to Gaussian deconvolution in the range 25000–5000 $cm^{-1}$ in order to detect the individual transitions (Figure 16). As is commonly observed, the bands show a slight shift on going from ambient to liquid-helium temperature and, therefore, equal band positions have not been enforced in the fit. The minimum number of Gaussian bands was used such that it is consistent with the experimentally observed peaks and shoulders yielding a total of 11 detectable transitions for neutral **1** below 25000 $cm^{-1}$ (bands 3–13 in Figure 16; see also Table 7).

The absorption spectrum is dominated by three reasonably intense transitions (bands 3, 5, and 8). A weaker band in between bands 3 and 5 and two weaker bands between 5 and 8 show up, and apparently there is a whole series of transitions to higher energy than band 8 that are not resolved in the absorption spectra, but lead to weak MCD features of variable sign. The temperature dependence of the MCD spectrum (not shown) indicates that all observed features arise from a *C*-term mechanism that is expected to dominate for paramagnetic molecules studied at low temperature. However, the *C*/*D* ratios of all bands (with the exception of band 4) are $\leq 0.01$, indicating that the MCD spectrum is at least not dominated by transitions of d–d character, which would require *C*/*D* ratios $\geq 0.03$. In particular bands 3 and 5, which are quite prominent in the absorption spectrum, have very small MCD intensities and the dominant absorption band 8 still only has a *C*/*D* ratio of 0.011.

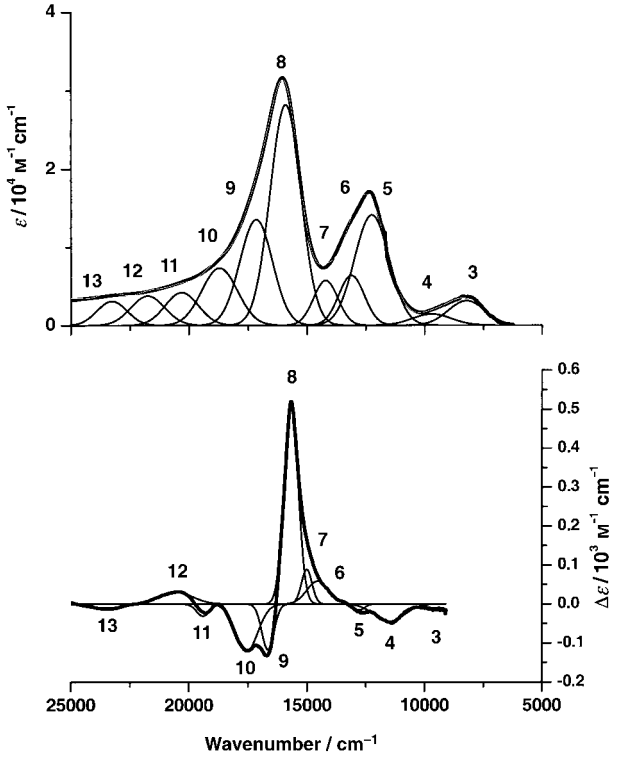


Figure 16. Deconvoluted electronic absorption spectrum $[Co(^1L_N)_2]^0$ (top) and its magnetic circular dichroism (MCD) spectrum (bottom) recorded at 1.8 K and 5.0 T.

These findings are consistent with the interpretation of the spectrum resulting from correlated ab initio calculations described below.

Of particular interest is the transition $1b_{1u} \rightarrow 2b_{2g}$, which corresponds to the LLCT transition of $A_u$ symmetry and is allowed in *x* polarization (along the long axis of the complex). In the case of the neutral cobalt complex this transition leads from a doubly occupied MO to a virtual MO (Figure 14). Thus, in the excited state there are three unpaired electrons that can spin couple to give two doublet and one quartet states. The absorption intensity for the quartet state will be very low since it is spin forbidden. Formally, the first doublet arises from the straightforward $1b_{1u} \rightarrow 2b_{2g}$ singlet excitation, while the second excitation involves the $1b_{1u} \rightarrow 2b_{2g}$ triplet excitation with a concomitant spin flip of the unpaired electron in the $2b_{3g}$ SOMO. Thus, the second doublet is referred to as a "trip-doublet" in Gouterman's nomenclature[36] and formally corresponds to a double excitation. However, the two doublets interact through the Hamiltonian operator and can, therefore, mix and acquire absorption intensity. From the SORCI calculations there is little doubt that bands 3 and 8 must be assigned to the two components of the $1b_{1u} \rightarrow 2b_{2g}$ transition, with the lower energy transition corresponding to the trip-doublet component. These transitions are calculated at 6175 and 12390 $cm^{-1}$ and observed at 8224 and 15927 $cm^{-1}$, respectively, which is considered to be good agreement. The calculated oscillator strengths of 0.006 and 0.359 are also in

  

Table 7. Detailed analysis of the optical transitions for **1** following Gaussian deconvolution of the experimental data shown in Figure 14 combined with the results of spectroscopy-oriented configuration interaction calculations.

| Band | Energy [cm$^{-1}$] exptl | calcd | Method[c] | Exptl $\bar{C}_0/\bar{D}_0$ | Oscillator strength exptl | calcd | Assignment |
|---|---|---|---|---|---|---|---|
| 1 | – | 1616 | abs | | – | 0.000 | $^2A_g(2a_g(d_{z^2})\rightarrow 2b_{3g}(d_{yz}))$ |
| 2 | – | 3789 | abs | | – | 0.001 | $^2B_{1u}(1b_{1u}(\pi^*)\rightarrow 2b_{3g}(d_{yz}))$ |
| 3 | 8224 | 6175 | abs | | 0.026 | 0.006 | $^2A_u(1b_{1u}(\pi^*)\rightarrow 2b_{2g}(\pi^*))$ |
| 4 | 9698 | 7983 | abs | | 0.012 | 0.000 | $^2B_{3u}(1b_{1u}(\pi^*),2a_g(d_{z^2})\rightarrow 2b_{3g}(d_{yz}),2b_{2g}(\pi^*))$ |
| | | 8552 | | | | 0.000 | $^2B_{2g}(1b_{2g}(d_{xz})\rightarrow 2b_{3g}(d_{yz}))$ |
| | 11384 | | MCD | −0.0240 | | | |
| 5 | 12245 | 11779 | abs | | 0.113 | 0.008 | $^2A_u(1b_{1u}(\pi^*),1,2a_g(d_{x^2-y^2},d_{z^2})\rightarrow 2b_{3g}(d_{yz}),1b_{1g}(d_{xy}))$ + $^2A_u(1b_{1u}(\pi^*),1,2a_g(d_{x^2-y^2},d_{z^2}),1b_{2g}(d_{xz})\rightarrow 2b_{3g}(d_{yz}),1b_{1g}(d_{xy}),2b_{2g}(\pi^*))$ |
| | 12788 | | MCD | −0.0004 | | | |
| 6 | 13112 | 12262 | abs | | 0.038 | 0.000 | $^2A_g(1a_g(d_{x^2-y^2})\rightarrow 2b_{3g}(d_{yz}))$ |
| | 14501 | | MCD | 0.0082 | | | |
| 7 | 14210 | [a] | abs | | 0.032 | | |
| | 15031 | | MCD | 0.0075 | | | |
| 8 | 15927 | 12390 | abs | | 0.200 | 0.359 | $^2A_u(1b_{1u}(\pi^*)\rightarrow 2b_{2g}(\pi^*))$ |
| | 15600 | | MCD | 0.0110 | | | |
| 9 | 17164 | 17482 | abs | | 0.100 | – | [b] |
| | 16654 | | MCD | −0.0040 | | | |
| 10 | 18704 | 18148 | abs | | 0.060 | – | [b] |
| | 17533 | | MCD | −0.0130 | | | |
| 11 | 20305 | 20033 | abs | | 0.032 | – | [b] |
| | 19290 | | MCD | −0.0036 | | | |
| 12 | 21746 | 21339 | abs | | 0.029 | – | [b] |
| | 20564 | | MCD | 0.0100 | | | |
| 13 | 23263 | [a] | abs | | 0.021 | – | [b] |
| | 23376 | | MCD | −0.0042 | | | |

[a] No transitions calculated. [b] Not analyzed. [c] abs = electronic absorption spectra, MCD = magnetic circular dichroism.

reasonable agreement with the experimentally determined values of 0.026 and 0.20, respectively, but it appears that the calculations underestimate the mixing of the two components somewhat thus leading to too low an intensity for the lower and a too large intensity for the upper state. The *C*/*D* ratio for the trip-doublet component is very low, as might be expected from its relatively large double excitation character, but the *C*/*D* ratio of band 8 approaches ~0.01. This shows that there must be considerable metal character involved in the acceptor orbital, since a pure, unipolarized LLCT transition should show a fairly weak MCD response.

In the SORCI calculations four states are calculated between bands 3 and 8; these results agree nicely with the four bands resolved in the simultaneous fit of the MCD and absorption spectra. The first of the intermediate states is dominated by the double excitation $^2B_{3u}(1b_{1u}(\pi^*),\ 2a_g(d_z{}^2)\rightarrow 2b_{3g}(d_{yz}),\ 2b_{2g}(\pi^*)$ at 7983 cm$^{-1}$, but with small absorption intensity owing to its two-electron nature. This double excitation is so exceptionally low-lying because the $2a_g(d_{z^2})\rightarrow 2b_{3g}(d_{yz})$ transition is very low in energy (vide infra); this in turn leads to considerable complexity in the calculated excited-state structure. However, this is characteristic of the coordinated radical species under investigation. The second transition calculated in the region of band 4 is the $^2B_{2g}(1b_{2g}(d_{xz})\rightarrow 2b_{3g}(d_{yz}))$ electric-dipole-forbidden "d–d" transition at 8552 cm$^{-1}$. Owing to the relatively large *C*/*D* ratio, this transition is likely to make the dominant contribution to band 4. The next intermediate transition is of complicated origin and is calculated at 11779 cm$^{-1}$ with an oscillator strength of 0.0079. We assign this transition to the reasonably intense band 5 observed at 12249 cm$^{-1}$. Its calculated symmetry is $^2A_u$, and it therefore can obtain considerable intensity from mixing with the intense LLCT band, which has the same symmetry. The origin of the experimentally observed intensity must arise from such mixing mechanisms, since the calculated origin of this band unexpectedly reveals that it is mainly composed of double (~50% $1b_{1u}(\pi^*)$, $1,2a_g(d_{x^2-y^2},d_{z^2})\rightarrow 2b_{3g}(d_{yz}),1b_{1g}(d_{xy})$) and even triple excitations (~25% $1b_{1u}(\pi^*),1,2a_g(d_{x^2-y^2},d_{z^2}),1b_{2g}(d_{xz})\rightarrow 2b_{3g}(d_{yz}),1b_{1g}(d_{xy}),2b_{2g}(\pi^*)$). The interpretation of band 5 results from the ab initio calculations; this could have hardly been anticipated in advance and demonstrates the importance of an unbiased multireference approach. In the present case the SORCI calculations include up to and including pentuple excitations from the leading ground state configuration and these high excitations are also required in order to properly capture the differential dynamic correlation effects.[37] It is evident from these considerations that any single reference treatment of the excited states of $[Co(^1L_N)_2]^0$ will be inflicted with large difficulties and is likely to lead to unbalanced results.

The final transition calculated below the intense band 8 is the electric-dipole-forbidden $^2A_g(1a_g(d_{x^2-y^2})\rightarrow 2b_{3g}(d_{yz}))$ "d–d" transition. It is calculated at 12262 cm$^{-1}$ and occurs in the region of bands 6 and 7 observed at 13112 and 14210 cm$^{-1}$, respectively. However, the case for two bands in this region is not unambiguous. The calculated oscillator strength is zero, but the transition may borrow intensity

from the near-lying, intense, allowed transitions by low-symmetry distortions and vibronic coupling effects. Beyond the intense band 8 the density of states increases and we have calculated additional states at 17482, 18148, 20033 and 21339 $cm^{-1}$ consistent with the appearance of bands 9–13, which occur in these regions. All of these transitions are of complicated nature and involve low-lying double excitations that were not further analyzed. Their MCD features are very weak.

The origin of the MCD intensities is subject to debate. In the $D_{2h}$ point group all transitions are unipolarized and, thus, spin-orbit coupling (SOC) to other states with non-collinear transition moments is required in order to obtain non-zero MCD intensity.[38] Since the SOC only couples states of like parity, it is either the SOC of the ground state with other "gerade" states or the coupling of electric dipole allowed states with other "ungerade" states that gives rise to the observed signs. Since in our interpretation the main intensity in the absorption spectrum arises from *x*-polarized $^2B_{3g}\rightarrow{}^2A_u$ transitions, the nature of the coupling states is not immediately evident. For the excited-state SOC mechanism, which gives rise to a sum rule,[38] the prime candidates are *y*-polarized $^2B_{1u}$ states of which we calculate only one at very low energy (vide infra) and with a low transition moment. It is, however, conceivable that other excited states of this symmetry that exist outside the studied spectral window significantly contribute to the observed MCD intensities. That such mechanisms are operative, at least in addition to the ground-state SOC mechanism, is witnessed by the fact that the spectrum is not strongly dominated by bands of only one sign, which is often the case if the ground-state SOC dominates the MCD response.

In the SORCI calculations, two additional very low-lying states were found that are outside the detection range of the absorption and MCD experiments. The first state corresponds to the $^2A_g(2a_g(d_{z^2})\rightarrow 2b_{3g}(d_{yz}))$ parity forbidden d–d transition, which is calculated to occur as low as 1616 $cm^{-1}$. Since this state spin-orbit couples to the ground state through the *x* component of the SOC operator, its very low energy nicely explains the very large $g_{max}$ shift observed for $[Co(^1L_N)_2]$ in the EPR experiments. A more detailed analysis of the ground-state magnetic properties of cobalt complexes within this family will be presented elsewhere. The second low-lying excited state corresponds to the $^2B_{1u}(1b_{1u}(\pi^*)\rightarrow 2b_{3g}(d_{yz}))$ electric-dipole-allowed LMCT transition, which is calculated at 3789 $cm^{-1}$ but with a fairly low oscillator strength of $9.3\times10^{-4}$.

The SORCI ab initio calculations lead to rather good agreement with the experimentally observed absorption spectrum of $[Co(^1L_N)_2]^0$ (the errors in the calculated transition energies do not exceed 0.2–0.3 eV). The calculations also reveal quite a high degree of electronic structure complexity, which we believe to require a multireference approach such as the SORCI method to be properly dealt with. The two intense peaks 3 and 8 are interpreted as the two components of a multiplet-split LLCT transition with the splitting approaching 1 eV; this type of splitting is only possible for strong intersite interactions. The remaining transitions are of LMCT and d–d origin. It is particularly interesting that the calculations predict a very low-lying excited d–d state below 2000 $cm^{-1}$ which is responsible for the very large $g_{max}$ shift observed in the EPR experiments.

The $[Co(^1L_N)_2]^-$ complex proved to be too unstable for the MCD measurements. Hence, we will skip the assignment of the transitions for the anion, since in the absence of the MCD it will not be possible to prove the validity of our assignments.

*Comparison of SORCI and DFT ground-state description*: We will now compare the calculated ground-state electron and spin distribution between the DFT and SORCI calculations. The first meeting point between DFT and correlated ab initio theory is the one-electron density. The comparison in terms of a Löwdin population analysis is meaningful, since both methods were carried out with the same basis set and geometry (Table 8).

Table 8. Comparison of the charge and spin populations at the cobalt ions resulting from a Löwdin analysis of the one-electron density of the ground state from ab initio SORCI and B3LYP density functional (in parentheses) calculations.

| | Electron d | Electron 4s | Spin d | Spin s |
|---|---|---|---|---|
| $[Co(^1L_N)_2]$ | 7.65 (7.64) | 0.43 (0.51) | 0.97 (1.14) | 0.07 (0.00) |
| $[Co(^1L_N)_2]^{1-}$ | 7.42 (7.60) | 0.54 (0.53) | 1.56 (1.47) | 0.00 (0.00) |

For the neutral species, the analysis shows a d population between seven and eight electrons and a spin density of essentially one unpaired electron at the central cobalt atom. Both values would be consistent with a central, low-spin $Co^{II}$ ion and this would also be in accord with the interpretation of the optical spectrum, which shows that essentially all intensity arises from the LLCT transition of the coordinating ligand in the diradical form. Thus, the ground state wavefunction would contain three open-shell $S=1/2$ fragments that are coupled to a total spin of $S_t=1/2$. In fact the SORCI many-electron ground-state wavefunction contains ~7% of the double excitation $(1b_{1u})^2\rightarrow(2b_{2g})^2$, which describes the diradical character of the ligand and rules out the alternative of ferromagnetic coupling between the ligands and antiferromagnetic coupling to the central metal. It is clear that such a complicated behavior can only be crudely modelled with DFT methods. In fact the DFT value of 1.14 unpaired electrons on the central cobalt and $\langle\hat{S}^2\rangle=0.83$ show a partial broken symmetry character in a "desperate" attempt of the variational principle to minimize the energy towards the truly multiconfigurational ground state; this is, however, impossible within the restrictions imposed by a single determinantal wavefunction.[39] In addition, the natural orbitals of the SORCI calculation show a relatively pure $d_{xz}$-based $b_{2g}$ orbital in contrast to the strong mixing observed in the DFT calculations and which made the oxidation state assignment ambiguous. Thus, from the point of

  

view of the SORCI calculations, the assignment of the spectroscopic oxidation state as $Co^{II}$ is the preferred one.

Interestingly, for the anionic species the d-orbital population at the central cobalt atom *decreases*, while the spin population *increases* to more than 1.5 unpaired electrons. Both observations would seem to indicate that the central cobalt is *oxidized* to a $Co^{III}$ ion with $S=1$ upon *reduction* of the complex, while the ligands would exist in the dianionic redox innocent form. This is also in accord with the interpretation of the structural data discussed above. However, both the d population (which is somewhat higher than expected for $Co^{III}$) and the spin population (which is lower than expected for $Co^{III}$) show that this description is oversimplified. Thus the actual electronic structure may be best described by the resonance forms $[Co^{III}(L^{2-})(L^{2-})]^- \rightleftarrows [Co^{II}(L^{\cdot-})(L^{2-})]^- \rightleftarrows [Co^{II}(L^{2-})(L^{\cdot-})]^-$, but with a somewhat larger weight for the first structure. The DFT results are also in accord with this interpretation, since the $\langle \hat{S}^2 \rangle$ value of 2.01 indicates little spin contamination or broken symmetry character and the calculated populations are in reasonable accord with the SORCI calculations, although the loss of metal d-based charge is less pronounced in the DFT case.

We conclude that multiconfigurational ab initio methods in form of the SORCI procedure successfully account for the experimental observations despite the fact that the electronic structure of the molecules investigated is very complicated. This work is perhaps among the first attempts to significantly go beyond the restrictions of DFT in the modeling of transition-metal radical systems and demonstrates that such approaches, despite their somewhat higher computational cost, have become increasingly feasible and, therefore, add a powerful new tool in the theoretical arsenal available to treat such systems. This is particularly true for the interpretation of the fascinating optical properties of such systems that are even more complicated than the already complicated ground states, and any method based on a single Slater determinant reference will have great difficulties to arrive at a successful interpretation.

## Discussion

In the Introduction we pointed out that small structural differences in the ligand C–N and C–C distances between the corresponding four-coordinate cobalt and nickel complexes may exist and might point to differing ligand oxidation levels (and concomitantly central metal ions) in the two neutral complexes and the corresponding one-electron reduced monoanions. This has been verified by low-temperature (100 K) crystallography of neutral **4** and **8** on the one hand and of **5** and **9** on the other. By using DFT and correlated ab initio calculations these differences were traced to energetic differences of the $2b_{2g}$ and $2b_{3g}$ orbitals relative to the metal d orbitals. As shown in Figure 15 in the nickel cases both orbitals are predominantly ligand-centered and the central nickel ion has a $d^8$ electron configuration of $Ni^{II}$ in four occupied metal d orbitals, the neutral, mono- and dianions and their electronic structures may be adequately represented by the following resonance structures:

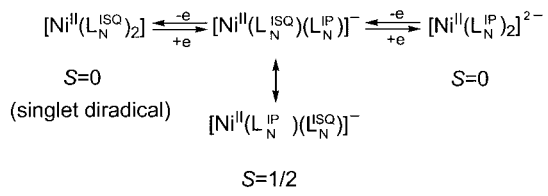


Very similar behavior is deduced for the series $[Ni(^4L_O)_2]^{n-}$ $(n=0,1,2)$. The electronic absorption spectra of the neutral and monoanionic species of nickel are dominated by a single intense band that is of ligand-to-ligand charge transfer character in the former and of intervalence charge transfer character in the latter. This band is absent in the dianionic form because the $2b_{2g}$ orbital is now filled (HOMO).

The four-coordinate cobalt complexes are more difficult to understand, even qualitatively, because the out-of-plane orbital $2b_{2g}$ has almost equal contributions from the Co $3d_{xz}$ and the $b_{2g}$ ligand fragment orbitals. It is therefore not possible to assign straightforwardly a spectroscopic oxidation state for the cobalt ion. On the other hand, it is clear that the one-electron oxidation of the monoanion leads to a *decrease* of the metal character of the $2b_{2g}$ orbital. Taking the following resonance structures into account one can describe the electronic structures as follows:

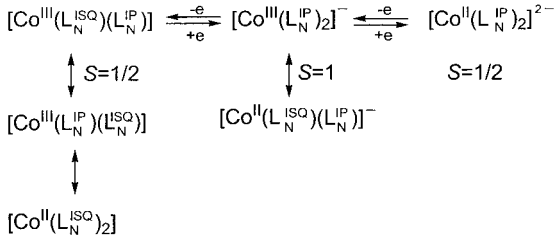


The resonance structures that formally contain $Co^{III}$ ions have significant weights which nicely explains the observed ligand bond lengths in four-coordinate complexes **1**, **4**, and **5**.

On first sight, it is somewhat counterintuitive that the addition of a fifth ligand, such as pyridine, to the four-coordinate species **1** to yield complex **2** does not change the electronic spectra (Figures 11 and 13), but alters the EPR spectra dramatically (Figure 12). However, these results are readily understood from the calculations presented above. Thus, an addition of a fifth ligand does not alter the electronic configuration at the central metal ion and consequently the number and nature of allowed electronic transitions remains conserved. In particular, it is the equatorial li-

gands that give rise to the observed absorption intensities and these are little affected by the presence of an additional axial ligand in the present case. That the electronic configuration at the central cobalt stays intact is witnessed by the presence of the trip-doublet feature[36] at ~1200 nm, which can only arise if there are three unpaired electrons in the excited state.

The EPR parameters are dominated by a different mechanism. Here the spin-orbit coupling of electric-dipole-forbidden states with the ground state determines the *g* shift (deviation from the free electron *g* value; $g_e = 2.0023$). In **1** the state that gives the dominant contribution to the $g_z$ value is in fact very low in energy ($< 2000\ cm^{-1}$ in our calculations) and involves a transition from the out-of-plane $d_{z^2}$ orbital into the $d_{yz}$-based SOMO. It is intuitively clear that the addition of a fifth ligand must indeed have a major effect on the position of this low-lying state. Thus, already a shift in the transition energy of a few thousand wavenumbers is able to explain the enormous reduction of the $g_z$ shift by almost a factor of three from 0.81 in **1** to a value of 0.31 in **2**. That subtle variations have a large influence on $g_z$ is also consistent with the large change of $g_z$ ($\Delta g_z \sim 0.3$) in going from **1** ($g_z = 2.81$) to the very similar species **4** ($g_z = 3.11$). Clearly, given the limited value of the one-electron SOC constant on Co ($\sim 600\ cm^{-1}$) $g_z$ values larger than 2.5 are only possible in the presence of near orbital degeneracy.

The monocationic form of $\mathbf{1}^+$ has not been structurally characterized, but it should possess an electronic structure such as $[Co^{III}(^1L_N^{ISQ})_2]^+$ or $[Co^{II}(^1L_N^{ISQ})(^1L_N^{IBQ})]^+$ with a singlet or triplet electron configuration $(1a_g)^2(2a_g)^2(1b_{3g})^2(1b_{2g})^2(1b_{1u})^1(2b_{3g})^1(2b_{2g})^0$ or $(1a_g)^2(2a_g)^2(1b_{3g})^2(1b_{2g})^2(1b_{1u})^2(2b_{3g})^0(2b_{2g})^0$. Upon five-coordination as in **2a**, **3**, and **7**, the $1b_{2g}$ orbital becomes predominantly metal-centered ($d_{xz}$). This leads to a closed-shell electron configuration $(1a_g)^2(2a_g)^2(1b_{3g})^2(1b_{2g})^2(1b_{1u})^2(2b_{3g})^0(2b_{2g})^0(1b_{1g})^0$ with a singlet ground state (as is observed) for a $d^6$ ($Co^{III}$) configuration. This would explain the structural ligand dimensions in **2a**, **3**, and **7** as two radical ions $(L_N^{ISQ})^{\bullet -}$ and their similar electronic spectra. It is interesting that similar electronic effects have been observed for three complexes containing the redox-innocent ligand *o*-phenylenebis(biuretate)(4−) (bbphen): the four coordinate species $[Co^{III}(bbphen)]^-$ possesses an $S = 1$ ground state, whereas the five- and six-coordinate species $[Co^{III}(bbphen)(CN)]^-$ and $[Co^{III}(bbphen)(CN)_2]^{3-}$ are both diamagnetic ($S = 0$).[32f]

It is here and previously clearly established that in complexes containing only one dioxolene-type ligand, namely $(^XL_N)^{0,1-,2-}$ or $(^XL_O)^{0,1-,2-}$, the respective oxidation level is defined by high-quality X-ray crystallography, because their C–O, C–N and C–C bond lengths are characteristic for a given oxidation state (see Figure 4). Therefore, we feel that in a series of crystallographically characterized ruthenium and osmium complexes reported by Goswami et al.[40–43] the assigned ligand and metal oxidation states as diimineruthenium(II) or diimineosmium(II) species are incorrect. The ligand dimensions clearly point to the presence of *o*-diiminosemiquinonato(1−) radicals: Thus $[Ru^{II}(acac)_2(^2L_N^{IBQ})]$ is in fact $[Ru^{III}(acac)_2(^2L_N^{ISQ})]$;[41] $[Ru^{II}Cl_2(PhNH_2)_2(^2L_N^{IBQ})]$ is $[Ru^{III}Cl_2(PhNH_2)_2(^2L_N^{ISQ})]$, and $[Ru^{II}Cl_2(bpy)(^2L_N^{IBQ})]$ is $[Ru^{III}Cl_2(bpy)(^2L_N^{ISQ})]$.[42] Interestingly, the complex formulated as $[Os^{II}Br_2(^2L_N^{IBQ})_2]$ should most probably be understood as a mixed-valent ligand class III species $[Os^{III}Br_2(^2L_N^{ISQ})(^2L_N^{IBQ})]$.[43] In $[Ru^{II}(bipy)_2(^2L_N^{IBQ})](PF_6)_2$ the metal and ligand oxidation states have been correctly assigned.[10]

## Acknowledgement

We thank the Max-Planck Society and the Fonds der Chemischen Industrie for financial support of this work.

[1] A.L. Balch, R. H. Holm, *J. Am. Chem. Soc.* **1966**, *88*, 5201.
[2] L. F. Warren, *Inorg. Chem.* **1977**, *16*, 2814.
[3] S.-M. Peng, C.-T. Chen, D.-S. Liaw, C.-I. Chen, Y. Wang, *Inorg. Chim. Acta* **1985**, *101*, L31.
[4] F. Cariati, F. Morazzoni, C. Busetto, G. Del Piero, A. Zazzetta, *J. Chem. Soc. Dalton Trans.* **1976**, 342.
[5] W. P. Schaefer, R. E. Marsh, *Acta Crystallogr. Sect. B* **1969**, *25*, 1675.
[6] C. Daul, C. W. Schläpfer, A. v. Zelewski, *Struct. Bonding* **1979**, *36*, 12.
[7] S. Nemeth, L. I. Simandi, G. Argay, A. Kálman, *Inorg. Chim. Acta* **1989**, *166*, 31.
[8] P.-H. Cheng, H.-Y. Cheng, C.-C. Lin, S.-M. Peng, *Inorg. Chim. Acta* **1990**, *169*, 19.
[9] a) D. Herebian, E. Bothe, F. Neese, T. Weyhermüller, K. Wieghardt, *J. Am. Chem. Soc.* **2003**, *125*, 9116; b) D. Herebian, K. E. Wieghardt, F. Neese, *J. Am. Chem. Soc.* **2003**, *125*, 10997.
[10] H.-Y. Cheng, C.-C. Lin, B.-C. Tzeng, S.-M. Peng, *J. Chin. Chem. Soc.* **1994**, *41*, 775.
[11] D. Herebian, P. Ghosh, H. Chun, E. Bothe, T. Weyhermüller, K. Wieghardt, *Eur. J. Inorg. Chem.* **2002**, 1957.
[12] P. Chaudhuri, C. N. Verani, E. Bill, E. Bothe, T. Weyhermüller, K. Wieghardt, *J. Am. Chem. Soc.* **2001**, *123*, 2213.
[13] P. Ghosh, A. Begum, D. Herebian, E. Bothe, K. Hildenbrand, T. Weyhermüller, K. Wieghardt, *Angew. Chem.* **2003**, *115*, 581; *Angew. Chem. Int. Ed.* **2003**, *42*, 563.
[14] X. Sun, H. Chun, K. Hildenbrand, E. Bothe, T. Weyhermüller, F. Neese, K. Wieghardt, *Inorg. Chem.* **2002**, *41*, 4295.
[15] C. N. Verani, S. Gallert, E. Bill, T. Weyhermüller, K. Wieghardt, P. Chaudhuri, *Chem. Commun.* **1999**, 1747.
[16] K. S. Min, T. Weyhermüller, K. Wieghardt, *Dalton Trans.* **2003**, 1126.
[17] L. S. Hegedus, in *Transition Metals in the Synthesis of Complex Organic Molecules*, University Science Books, Mill Valley, California **1994**, p. 3.
[18] C. K. Jörgensen, in *Oxidation Numbers and Oxidation States*, Springer, Berlin, Heidelberg, New York, **1969**.
[19] SHELXTL V.5, Siemens Analytical X-Ray Instruments, Inc., Madison, Wisconsin (USA), **1994**.
[20] SADABS, G. M. Sheldrick, University of Göttingen (Germany), **1994**.
[21] SHELXL97, G. M. Sheldrick, University of Göttingen (Germany), **1997**.
[22] F. Neese, Orca, an ab initio, DFT, and Semiempirical Electronic Structure Package, Version 2.2, Revision 74, Max-Planck-Institut für Bioanorganische Chemie, Mülheim an der Ruhr (Germany), June **2003**.
[23] A. D. Becke, *J. Chem. Phys.* **1986**, *84*, 4524.
[24] J. P. Perdew, *Phys. Rev. B* **1986**, *33*, 8522.
[25] a) A. Schäfer, H. Horn, R. Ahlrichs, *J. Chem. Phys.* **1992**, *97*, 2571; b) A. Schäfer, C. Huber, R. Ahlrichs, *J. Chem. Phys.* **1994**, *100*, 5289.

  

[26] Basis sets were obtained from the ftp server of the quantum chemistry group at the university of Karlsruhe (Germany) under http://www.chemie.uni-karlsruhe.de/PC/TheoChem/.
[27] a) P. Pulay, *Chem. Phys. Lett.* **1980**, *73*, 393; b) P. Pulay, *J. Comput. Chem.* **1992**, *13*, 556.
[28] C. Lee, W. Yang, R. G. Parr, *Phys. Rev. B* **1988**, *37*, 785.
[29] A. D. Becke, *J. Chem. Phys.* **1993**, *98*, 5648.
[30] F. Neese, *J. Chem. Phys.* **2003**, *119*, 9428.
[31] P. J. van der Put, A. A. Schilperoord, *Inorg. Chem.* **1974**, *13*, 2476.
[32] a) S. W. Gordon-Wylie, E.L. Bominaar, T. J. Collins, J. M. Workman, B.L. Claus, R. E. Patterson, S. E. Williams, B. J. Conklin, G. T. Yee, S. T. Weintraub, *Chem. Eur. J.* **1995**, *1*, 528; b) S. W. Gordon-Wylie, B.L. Claus, C. P. Horwitz, Y. Leychkis, J. M. Workman, A. J. Marzec, G. R. Clark, C. E. F. Rickard, B. J. Conklin, S. Sellers, G. T. Yee, T. J. Collins, *Chem. Eur. J.* **1998**, *4*, 2173; c) J. J. Bour, P. T. Beurskens, J. J. Steggarda, *J. Chem. Soc. Chem. Commun.* **1972**, 221; d) T. J. Collins, R. D. Powell, C. Slebodnick, E. S. Uffelman, *J. Am. Chem. Soc.* **1991**, *113*, 8419; e) J. C. Brewer, T. J. Collins, M. R. Smith, B. D. Santarsiero, *J. Am. Chem. Soc.* **1988**, *110*, 423; f) T. Yagi, H. Hanai, T. Komorita, T. Suzuki, S. Kaizaki, *J. Chem. Soc. Dalton Trans.* **2002**, 1126.
[33] a) N. Bresciani-Pahor, L. Randaccio, W. Summers, P. J. Toscano, *Inorg. Chim. Acta* **1983**, *68*, 69; b) M. F. Summers, L. G. Marzili, N. B. Bresciani-Pahor, L. Randaccio, *J. Am. Chem. Soc.* **1984**, *106*, 4478; c) S. J. Moore, R. J. Lachicotte, S. T. Sullivan, L. G. Marzili, *Inorg. Chem.* **1999**, *38*, 383; d) N. B. Pahor, S. Geremia, C. Lopez, L. Randaccio, E. Zangrando, *Inorg. Chem.* **1990**, *29*, 1043.
[34] C. R. Ollis, D. Y. Jeter, W. E. Hatfield, *J. Am. Chem. Soc.* **1971**, *93*, 547.
[35] S. E. Shadle, B. Hedman, K. O. Hodgson, E. I. Solomon, *J. Am. Chem. Soc.* **1995**, *117*, 2259.
[36] a) M. G. Cory, M. C. Zerner, *Chem. Rev.* **1991**, *91*, 813; b) M. Gouterman, *J. Mol. Spectrosc.* **1961**, *6*, 138.
[37] Differential dynamic correlation effects are represented by those parts of the dynamic correlation that change between different electronic states and are therefore essential for the calculation of accurate transition energies. As shown in the pioneering work of Malrieu, Caballol and co-workers (J. Miralles, J. P. Daudey, R. Caballol, *Chem. Phys. Lett.* **1992**, *198*, 555; J. Miralles, O. Castell, R. Caballol, J. P. Malrieu, *Chem. Phys. Lett.* **1993**, *172*, 33) a substantial part of the total dynamic correlation, namely the part which is brought in by the inactive double excitations, is expected to be nearly state independent. It is therefore the differential dynamic correlation that is the focus of the SORCI method, which may be viewed as an approximation to the iterative difference dedicated configuration interaction methodology (V. M. Garcia, O. Castell, R. Caballol, J. P. Malrieu, *Chem. Phys. Lett.* **1995**, *238*, 222).
[38] F. Neese, E. I. Solomon, *Inorg. Chem.* **1999**, *38*, 1847.
[39] F. Neese, *J. Phys. Chem. Solids* **2004**, *65*, 781.
[40] C. Das, S. Goswami, *Comments Inorg. Chem.* **2003**, *24*, 137.
[41] a) K. N. Mitra, P. Majumdar, S.-M. Peng, A. Castineiras, S. Goswami, *Chem. Commun.* **1997**, 1267; b) K. N. Mitra, S. Choudhury, A. Castineiras, S. Goswami, *J. Chem. Soc. Dalton Trans.* **1998**, 2901.
[42] C. Das, K. K. Kamar, A. K. Ghosh, P. Majumdar, C.-H. Hung, S. Goswami, *New J. Chem.* **2002**, *26*, 1409.
[43] a) K. N. Mitra, S. Goswami, *Chem. Commun.* **1997**, 49; b) K. N. Mitra, S. Goswami, *Inorg. Chem.* **1997**, *36*, 1322.

Received: August 17, 2004
Published online: November 17, 2004